University of Alberta

Annihilation of cardiac alternans by electric and mechano-electric feedback (MEF) in a cardiac tissue

by

Dipen Deshpande

A thesis submitted to the Faculty of Graduate Studies and Research
in partial fulfillment of the requirements for the degree of

Master of Science
in
Process Control

Department of Chemical and Materials Engineering

©Dipen Deshpande
Fall 2011
Edmonton, Alberta

Permission is hereby granted to the University of Alberta Libraries to reproduce single copies of this thesis and to lend or sell such copies for private, scholarly or scientific research purposes only. Where the thesis is converted to, or otherwise made available in digital form, the University of Alberta will advise potential users of the thesis of these terms.

The author reserves all other publication and other rights in association with the copyright in the thesis and, except as herein before provided, neither the thesis nor any substantial portion thereof may be printed or otherwise reproduced in any material form whatsoever without the author's prior written permission.

Abstract

Alternans occur prior to ventricular fibrillation and is a medical condition of heart that leads to sudden cardiac death (SCD). The presence of the electrical alternans induces, through the mechanism of the excitation-contraction coupling, an alternation in the heart muscle contractile activity. This work provides a study on the cardiac alternans annihilation by applied electrical and mechanical perturbation. In particular, we address annihilation of alternans in medically relevant size heart tissue by considering modulation of ionic currents in Luo-Rudy-1 (LR1) cardiac cell model, in which the control algorithm involves a combined electrical boundary pacing control and a spatially distributed calcium based control which perturbs the calcium in the cells. A parabolic partial differential equation (PDE) which is adapted from the ionic model is investigated to get an insight in terms of the controllability and stabilizability of the tissue for the suggested control input. Complimentary to this, we also address a novel mechanism of alternans annihilation which uses a Nash-Panfilov model coupled with the stress equilibrium equations. The coupled model includes an additional variable to represent the active stress which defines the mechanical properties of the tissue and is utilized in the feedback algorithm as an independent input from the pacing based controller realization in alternans annihilation.

“Dedicated to my supervisor, family, friends and my niece Navya- Diep ”

Contents

List of Figures

Chapter 1

Introduction

1.1 Motivation

Annually, about 30,000 - 40,000 of deaths occur due to sudden cardiac arrest (Billman, 2009). Ventricular fibrillation (VF) and ventricular tachycardia (VT) are types of arrhythmias known to be one of the primary reasons in majority of deaths due to cardiac arrest (Billman, 2009, Burke & Virmani, 2005). VF and VT are conditions associated with the abnormal electrical activity in the heart. Studies suggest that alternans are precursors to these life-threatening arrhythmias (Makarov & Komoliatova, 2010, Narayan, 2007, Pastore et al., 1999a). Alternans is a phenomenon observed in cardiac cells, in which the cells exhibit beat to beat alteration in the action potential duration (APD) when paced at short pacing intervals. The cardiac cells exhibit alterations as long(L)-short(S)-long(L)-short(S)-pattern in APD (see Fig.1.1). Under shorter pacing intervals these alternans sequentially develop into discordant alternans, conduction block (a condition in which the excitation induced beat that is unable to propagate in a cardiac tissue), reentrant propagation and initiating into a ventricular fibrillation (Pastore et al., 1999a). The action potential in cardiac tissue is associated with the contractile properties of the tissue so that physically alternans are manifested as an alteration in ability of the cardiac tissue to produce complete contraction and effectively push the ventricular blood volume in the body. Since alternans have been associated with the onset of ventricular fibrillation, it is important to explore whether spatiotemporal alternans in cardiac tissue can be annihilated in principle as the annihilation can represent an effective strategy to stabilize heart arrhythmias in order to prevent sudden cardiac death (SCD).

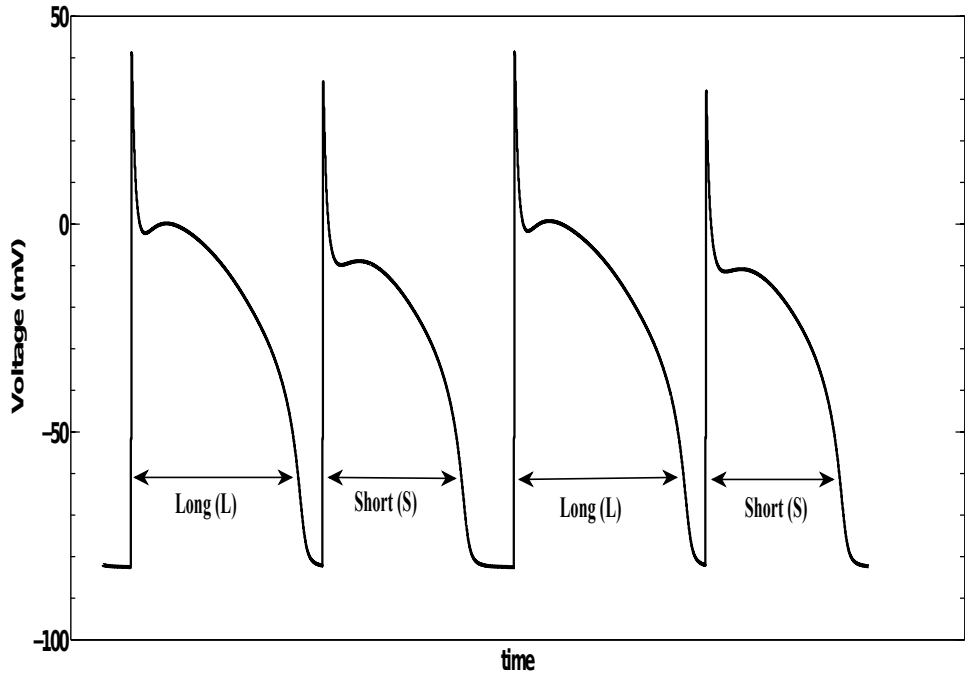

Figure 1.1: Time evolution of transmembrane voltage showing alternans in a single cell based on LR1 ionic currents.

1.2 The Control Problem

Currently, in order to correct pacing irregularities in heart and arrhythmias, electrical shocks delivered by specialized devices. An artificial pacemaker is one such device that applies an electrical shock, supporting the heart's natural pacemaker. The pacemaker has electrodes attached to a point in heart tissue that provides a low energy electrical shock with a desired frequency to correct certain irregularities in heart beat like bradycardia. An implantable cardiac defibrillator (ICD) is an advanced medical device used in patients prone to recurrent VF. Fig.1.2 shows the typical placement and electrode positioning of ICD (or pacemaker) unit in a human chest. An ICD is capable of delivering shocks of higher energy (as compared to pacemakers) to deal with complex arrhythmias (VT and VF). These high energy pulses delivered by an ICD last for very short time but are painful and possibly cause damage to the tissue. Newly developed ICDs are incorporated with algorithms to include anti-arrhythmogenic strategies. Hence, currently used ICD's can be used to incorporate strategies to annihilate alternans. This implies delivering lower energy shocks avoiding

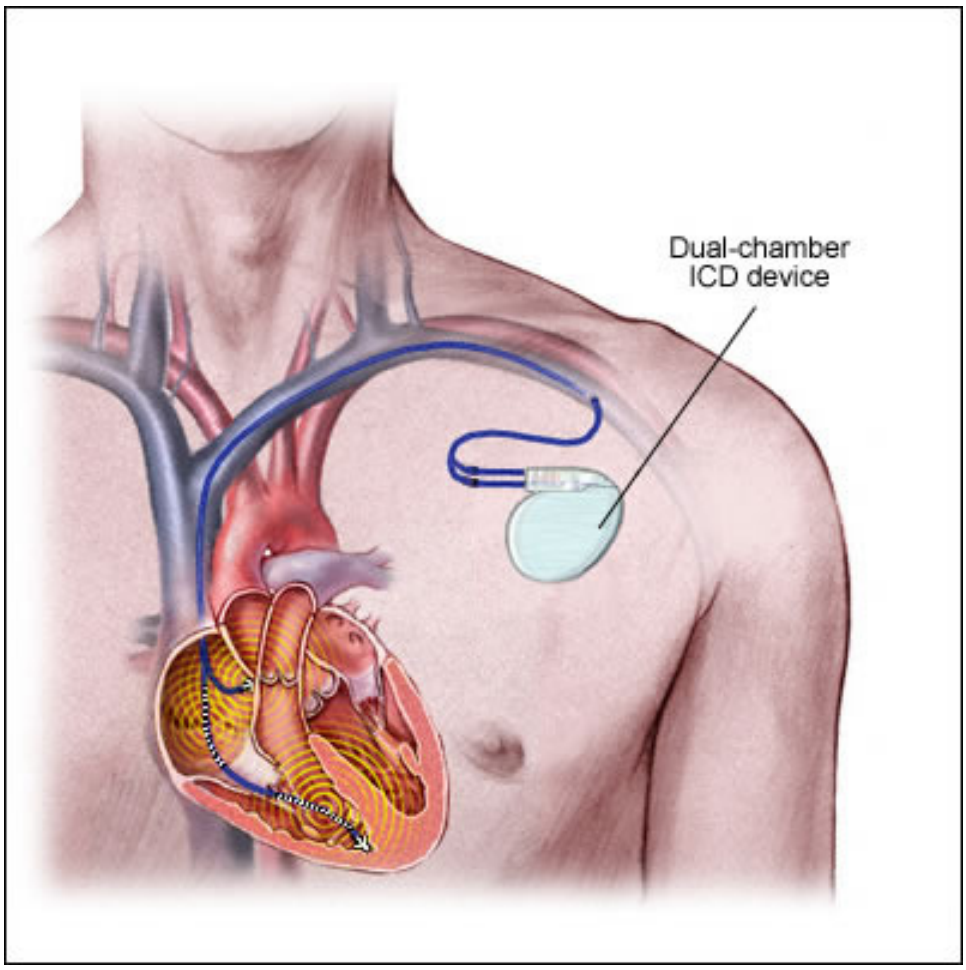

Figure 1.2: Implantable Cardiac Defibrillators (ICD).

painful shocks and trauma to the patients. Currently developed algorithms to annihilate alternans are based on electrical pacing that modulate the pacing interval at the boundary of the tissue. Such an electrical or boundary pacing control can successfully annihilate alternans in a single cell (Pastore et al., 1999a, Fox et al., 2002, Christini et al., 2006). However, recent theoretical and experimental studies (Pastore et al., 1999a, Fox et al., 2002, Christini et al., 2006, Echebarria & Karma, 2002) suggest that such electrical pacing control applied at the boundary of a cardiac tissue has finite controllability ($\approx 1cm$), and real time alternans control realizations (Lin & Dubljevic, 2007, Dubljevic et al., 2008) cannot stabilize alternans in cardiac tissues exceeding $\approx 1cm$ in length. Obviously, the stabilization of single cell alternans is easily realized compared to the alternans annihilation in the cable of cardiac cells or in the case of 2D or 3D tissue. Boundary pacing based control algo-

rithms, are realized by pacing at the boundary of the cardiac tissue which modulates the pacing interval based on the consecutive APDs at the pacing site (Christini et al., 2006). This control algorithm's failure to annihilate alternans completely in tissues exceeding $1cm$ length, is due to the lack of information of the evolution of alternans away from the pacing site to be effectively included in non-model based feedback algorithm. Moreover, the perturbation of pacing cycle length has intrinsic limitation due to the possibility of a conduction block. This limitation with electrical boundary pacing based controllers emphasize the need to look for electrical stimulus-independent techniques to annihilate alternans in medically relevant cardiac size tissue.

In a cardiac cell, along with the electrical activity there is an associated mechanical contraction and relaxation termed as the electro-mechanical or excitation-contraction coupling. When a cell excited it undergoes depolarization, the $[Ca^{2+}]$ ions are released via the calcium induced calcium release (CICR) mechanism. This released $[Ca^{2+}]$ ions binds with contractile proteins, mainly troponin C to induce cell contraction (Fig.1.3). This forms the features of electro-mechanical or excitation-contraction coupling. It has been shown that there also exists a reverse interaction between mechanical and electrical activity of the cardiac tissue (Kohl et al., 1999, Solovyova et al., 2004) wherein a mechanically induced stretch affects the electrical activity in heart. Calaghan et al., 2003 have experimentally shown that an axial stretch in the direction of the fibre causes the APD to prolong, showing the effect of a mechanical perturbation on the electrical species in heart. To overcome the limitation of finite controllability of controller algorithms based on electrical pacing based techniques, a mechanical stimuli based algorithm that is completely independent of electrical pacing has been investigated in this work.

Mechanical stimulus is usually applied to a cardiac cell in form of prod or a stretch. Through the mehano-electric coupling this stimuli influences the electrical activity in the cell which in turn affects the APD. In mechano-electric feedback system calcium is the most important ionic species that modulates the coupling in the cardiac cells (Bers, 2002), so that beat-to-beat variations in electric wave are linked to the alteration in the transient calcium concentration in cell (Chudin et al., 1998). Muscle stretch or shortening affects the myocardium which influences the shape and amplitude of the intracellular Ca transient (Calaghan et al., 2003).

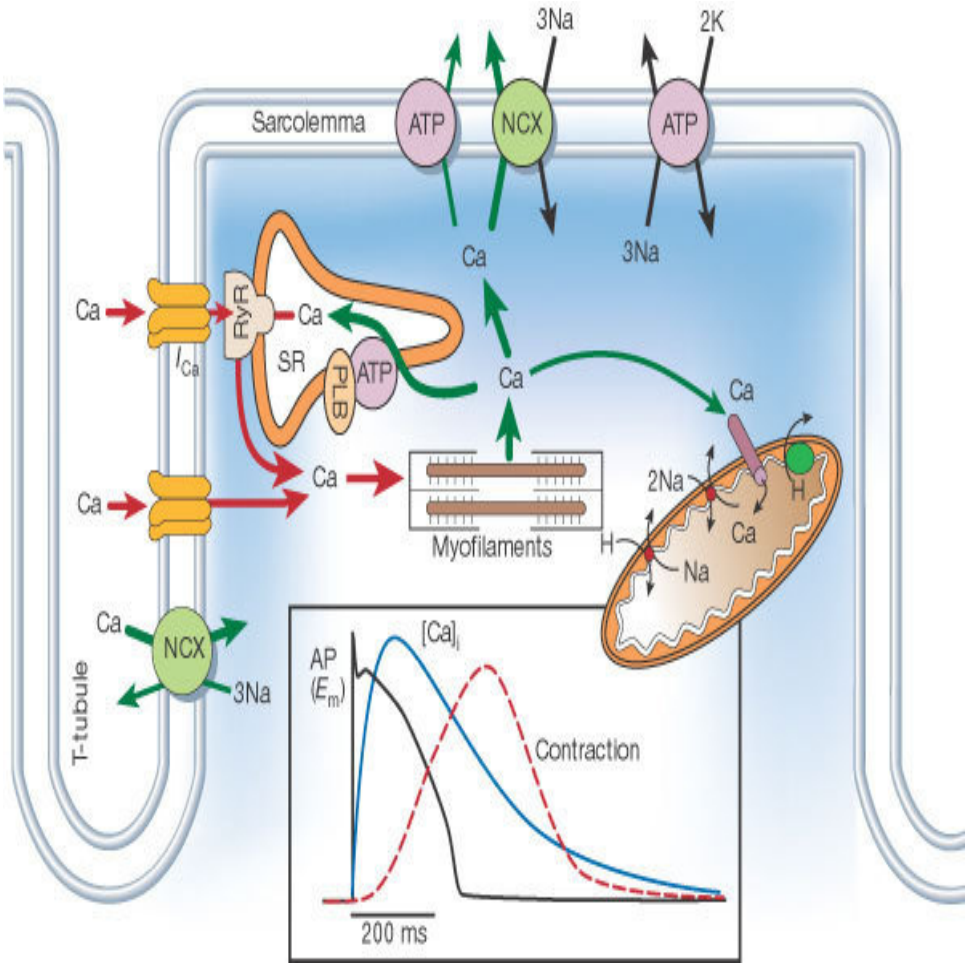

Figure 1.3: Ca^{2+} movement in the cell.

1.3 Thesis Contribution

Theoretical and experimental studies (Pastore et al., 1999b, Christini et al., 2006, Fox et al., 2002) on alternans annihilation have used the cardiac cell ionic model in 1D tissue and the associated small amplitude of alternans parabolic partial differential equation (PDE) (Echebarria & Karma, 2002). The ionic model of 1D cardiac cells provides a realistic model of a stripe of a cardiac tissue for control and stabilization alternans. A parabolic PDE model of a 1D cardiac tissue is a reaction-diffusion model associated with the complex ionic dynamics. With a parabolic PDE model it is possible to accurately determine the stabilizability of the system by determining the controllability of unstable modes. The spatial differential operator in the PDE system can be characterized by a spectrum that can be partitioned into a finite slow component and an infinite dimensional stable fast complement

(Friedman, 1976). Therefore, the control problem is reduced to, determine the controllability and further stabilization (if possible) of the unstable modes. The infinite dimensional stable part remains invariant under the applied feedback structure. The PDE model can be realized into a state space model for which a standard state feedback control structure using pole placement and/or optimal control techniques can be employed to stabilize the system (Curtain, 1982, Ray, 1981).

This work considers a control protocol involving mixed electrical boundary pacing control and a spatially distributed calcium based controller for stabilization of alternans in 1D cardiac ionic model tissue. We demonstrate alternans suppression via mechano-electric feedback in both the 1D cardiac cell ionic model and the associated amplitude of alternans linearized parabolic PDE model. In this study we suggest a control method that employs a spatial distributed calcium controller along with a electrical boundary pacing controller to address the limited controllability of having only an electrical pacing controller in a medically relevant sized cardiac tissue. We discuss the annihilation of alternans by the suggested control protocol both in a ionic and a PDE based model and show that results obtained from both models are in close agreement with each other. Further to corroborate these results, simulations are carried using simple three variable Nash-Panfilov model which has coupled mechanical stress and strain variable. This model is investigated for alternans stabilizations by employing direct mechanical perturbations in the feedback.

Chapter 2

Control of Alternans

In this chapter, the effect of proposed control protocol involving mixed electrical boundary pacing and a spatially distributed controller on stabilization of alternans is investigated. To determine the feasibility of such a control protocol experimentally, one needs a live cardiac tissue and also the experimental costs are high. Hence, computer based models are used to simulate a cardiac tissue and control techniques are applied. Two models are considered in this study: 1) Luo-Rudy 1 (LR1) model which has the electrical properties dependent on majority of relevant ionic currents flowing across a membrane of a real cardiac cell (Luo & Rudy, 1991) and associated with cardiac cell ionic model and 2) A PDE model suggested by (Echebarria & Karma, 2002, Shiferaw & Karma, 2006) which provides an analytical and qualitative insight in terms of the alternans controllability in the tissue and control algorithm ability to annihilate alternans.

2.1 Introduction to Ionic Models

A cardiac cell is a type of excitable medium. A cell is said to be excitable if a sufficiently large applied stimulus causes the cell membrane to go through an upstroke in voltage called the depolarization, which then repolarizes to the rest condition. The time length for which the cell is excited is termed as the action potential duration (APD). In cardiac cells the rest condition is termed as the diastole and the excited state as systole. Based on the formalism introduced by Hodgkin and Huxley (Hodgkin, 1952) a cell membrane can be modelled as a capacitor in parallel with an ionic current given as:

$$C_m \frac{dV}{dt} + I_{ion}(V,t) = 0 \tag{2.1}$$

Depending on the current I_{ion} complexity various models are developed.

2.1.1 FitzHugh-Nagumo Model (FHN)

The FHN model (FitzHugh, 1961) is a simpler form of the Hodgkin-Huxley model with only two variables. The model separates the behaviour of Hodgkin-Huxley model into a fast variable (v) and slow recovery variable (w). The fast variable consists of a cubic nullcline and the slow recovery variable has monotonically increasing nullcline. The governing equations are given as:

$$C_m \frac{dv}{dt} = f(v,w) + I_{stimulus} \tag{2.2}$$

$$\frac{dw}{dt} = g(v,w)$$

where the nullcline $f(v,w) = 0$ is cubic shaped and $g(v,w)$ is monotonically increasing.

$$f(v,w) = (a-v)(v-1)v - w$$
$$g(v,w) = \varepsilon(\beta v - \gamma w - \delta)$$

where a, ε, β, γ and δ are constants.

2.1.2 Noble Model

The Noble model (Noble, 1962) is a modified version of the Hodgkin-Huxley model developed for Purkinje fibres. Purkinje fibres are specialized myocardial tissues that are located below the endocardium in the inner walls of the heart that are responsible for propagation of electric charge and heart contraction. Noble model was the first model to describe a cardiac cell. The model suggests the I_{ion} to be dependent on the sodium current I_{Na}, potassium current I_K and anion current I_{An}. Hence, the model consists of four variables: voltage (V) and currents I_{Na}, I_K, I_{An}. The currents are further dependent on the respective ionic

conductances. At lower pacing rates the Noble model shows alternation in action potential and the bifurcation in the restitution curve (see Section.2.2.1 for information on restitution curve). It also predated the presence of calcium channels in cardiac cells.

2.1.3 Beeler-Reuter model

The Beeler-Reuter model (Beeler & Reuter, 1977) has been developed based on the ionic currents I_{ion} obtained from experimental work on a mammalian ventricular myocardium tissue. These include the fast inward sodium current I_{Na}, secondary or slow inward current I_s carried mainly but not exclusively by calcium ions, time activated outward current I_{x1} primarily due to potassium ions and time independent potassium current I_K. The model could indicate the importance of fast inward sodium current I_{Na} during the depolarization phase or the initial upstroke in the action potential. Based on the experimental data, the model could very well reconstruct features related to currents I_s, I_K and I_{x1}. The model suggested that the repolarization of the action potential is due to the decrease in slow inward current I_s and increase in time-dependent outward current I_{x1}. In most cases, the dominant factor is decrease in I_s, however in repetitive fast pacing the build up of I_{x1} is responsible for the shortening of APD.

2.1.4 Luo-Rudy model phase 1(LR1)

The LR1 model (Luo & Rudy, 1991) is a modified version of the Beeler-Reuter model with parameters determined on experimental findings based on availability of advanced voltage clamp techniques. The model is capable of reconstructing the depolarization characteristics in accordance with the experimental findings. The model describes the current I_{Na} to be inactivated by two processes - fast and slow. Current I_{Na} is characterized by large channel conductance resulting in a fast excitation or upstroke in action potential resulting into a membrane rate of depolarization $(\dot{V}_{max} = 400V/sec)$ which is three times larger than the Beeler-Reuter model and is in good agreement with the experimental data from mammalian ventricular cells. With a faster depolarization rate the model incorporates a slower I_{Na} inactivation which ensures slower recovery from excitability. It also includes a potassium channel that activates at higher potential and is incorporated in the current I_{K1}. The model describes the dependence of I_K and I_{K1} on extracellular potassium concentration $[K]_o$. Thus

LR1 model includes majority of the currents flows across a cell membrane and describes the depolarization and repolarization characteristics that are in good agreement with the experimental findings, at the same time the model is computationally not very complex as compared to the models that followed it. Hence, for the scope of this study, LR1 model is quiet appropriate. Fig.2.1 shows the electrical activity in a single cardiac cell simulated using ionic currents as suggested in LR1 model. The figure shows two beats in a cardiac cell due to the excitation by electrical stimulus provided.

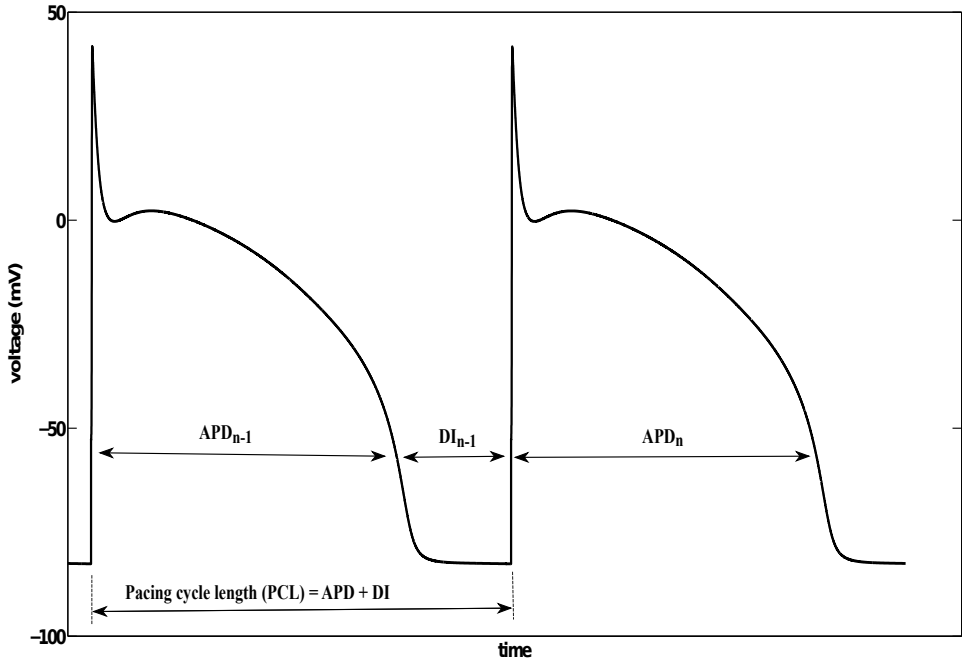

Figure 2.1: Time series plot showing the electrical activity in a single cardiac cell using LR1 ionic model.

2.1.5 Luo-Rudy dynamic model-1 (LRd-1) and Luo-Rudy dynamic model-2 (LRd-2)

LRd-1 (Luo & Rudy, 1994a) and LRd- 2 (Luo & Rudy, 1994b) are extensions of the LR1 model (Luo & Rudy, 1991). It includes a more detailed description of the processes regulating the intracellular Ca^{2+} concentration. The process that regulate Ca^{2+} concentration are stated as $Na^{+} - K^{+}$ pump, $Na^{+} - Ca^{2+}$ exchanger, a non-specific Ca^{2+} - activated current

a Ca^{2+} pump in the sarcolemma, uptake and release of Ca^{2+} in the sarcoplasmic reticulum (SR) and buffering of Ca^{2+} in myoplasm and SR.

2.2 Numerical Analysis and control of alternans in LR1 model of cardiac cell

First, we consider a computer simulated single cell control of cardiac alternans. Second, a computer simulated cardiac tissue in one-dimension is considered to test the credibility of the suggested control algorithm to suppress the alternans. Ionic currents suggested in LR1 model (described in Sec.(2.1.4)) are used to simulate the cardiac tissue numerically.

2.2.1 Alternans

As discussed earlier alternans is a condition when the width of the electric wave in the cells alternates. The phenomenon of alternans itself is quiet robust, i.e. the cardiac tissue is able to recover from alternans that are small in amplitude. But at a certain critical pacing frequency or interval (CPI) sustained alternans are induced. If such sustained alternations in a cardiac tissue are not controlled or suppressed they might lead to a conduction block (Fig 2.9) and cardiac arrhythmias (VT and VF). To relate the alternans of the single cell to the tissue behaviour, the effect of alternans can be described based on the Frank-Starling mechanism or Starling's law of heart which states that the output of the heart is equal to and determined by the blood flowing into the heart, and may be increased or diminished within very wide limits according to the inflow (Patterson, 1914, Starling, 1918). Increased volume of blood stretches the ventricular wall, causing cardiac muscle to contract more forcefully. Therefore, a strong beat leaves a small residual end-systolic volume reducing the end-diastolic volume and hence a reduced force development. The end of an action potential is followed by a finite time interval before the next action potential known as the diastolic interval (DI), which is required by the ventricles to fill with blood (diastolic filling) after a contraction, before the next activation. In case of the single cell and/or tissue, under a CPI pacing, the cells of the ventricles due to lack of time, fill to a lower capacity volume and hence leads to a short APD (refer Fig.1.3 and Fig.2.1). Thus, the action potential duration is dependent on the diastolic time.

$$APD_{n+1} = f(DI_n) \tag{2.3}$$

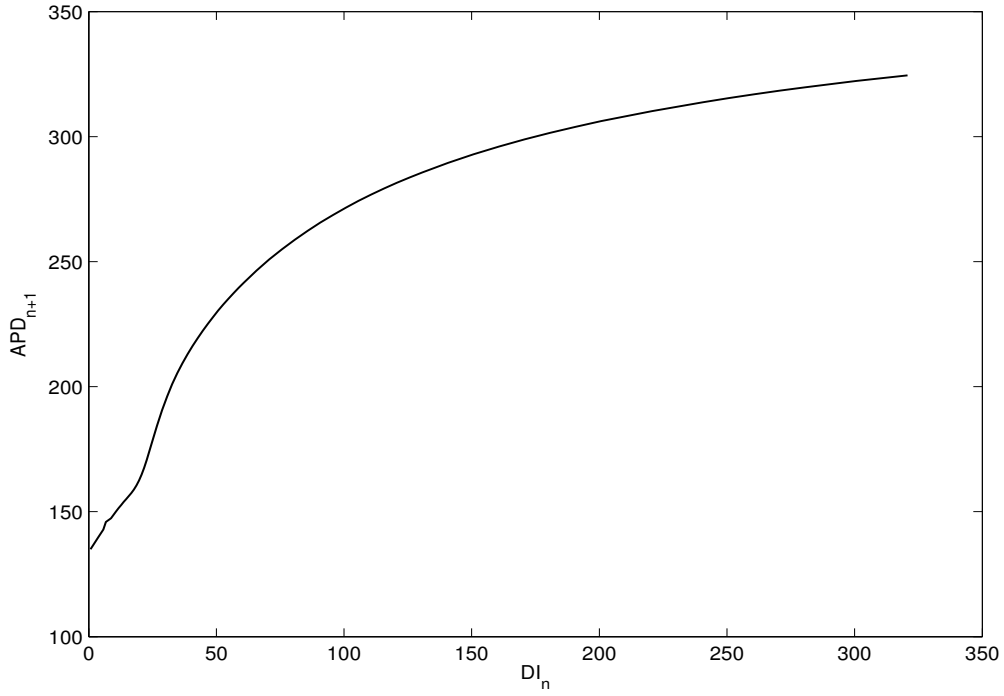

Figure 2.2: Restitution Curve.

Above defined relationship is represented graphically by a restitution curve (Fig.2.2). The S1S2 protocol is used to develop the restitution curve describing the APD and DI map (refer Sec.2.2.1). From restitution curve, it can be seen that the APD is unaffected by the change in DI for higher DI values with slopes approximately zero but for low DI (faster pacing intervals) the curve becomes steeper. Hence, the APD has a increasing dependence on DI at lower DI values and is constant at higher pacing periods. The presence of alternans corresponds to the point on the curve where slope is equal to or greater than unity. The unstable nature of alternans can be explained by the Cob-Web diagram (see Fig.2.3). On the Cob-Web diagram the solid-blue line represents $\text{APD}_{n+1} = f(\text{APD}_n)$ and the dashed-red as $\text{APD}_{n+1} = \text{APD}_n$. The point of intersection of these two lines represent absence of alternans in the cell i.e $\text{APD}_{n+1} = \text{APD}_n$. When the slope of restitution curve is < 1 the cardiac cell due its robust nature to stabilize alternans moves towards a stable point where

as, when the PCL is very short such that the slope of restitution curve is ≥ 1, the cardiac cell looses its ability to stabilize by itself and shows sustained alternans with increasing amplitude.

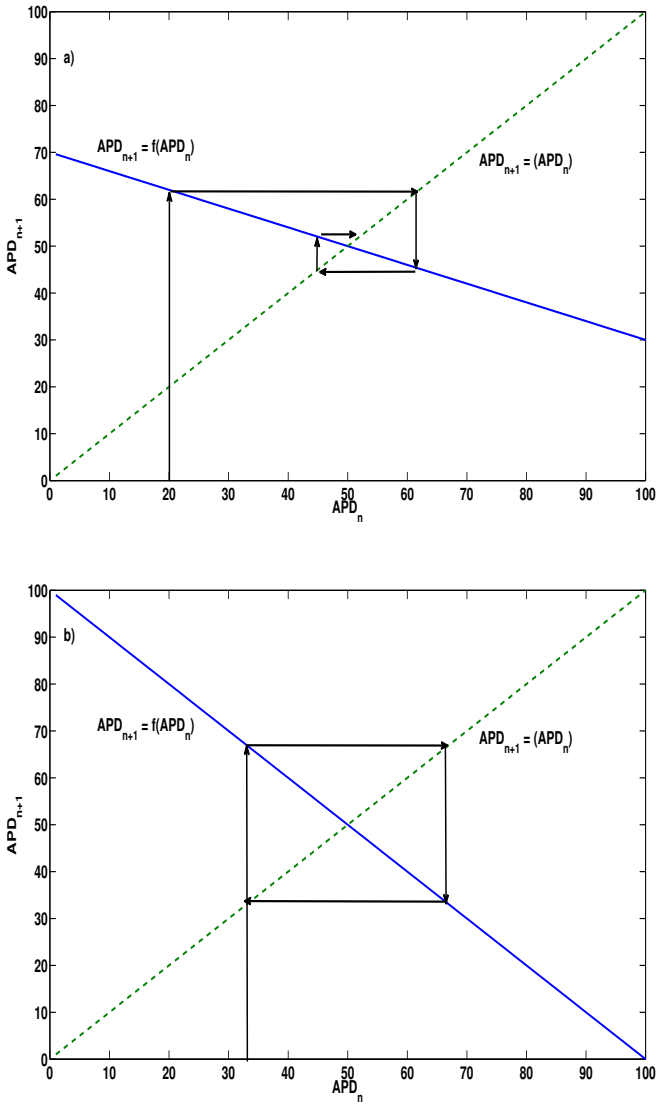

Figure 2.3: Cob-web diagrams showing the nature of alternans. a) Shows the ability of a cardiac cell to stabilize alternans by itself when the slope of restitution curve is < 1; b) When the slope of the restitution curve is ≥ 1, the systems drives away from the point of intersection (no alternans) to a unstable state.

S1S2 protocol

The single cell is given an electrical stimuli at sufficiently large pacing cycle length (PCL_{S1}) for 50 beats, where the last in series is termed S1. This S1 is followed by a S2 stimuli having a shorter PCL_{S2} than S1, which is able to produce an action potential. For a range of PCL_{S2} values that are shorter than PCL_{S1} the APD and DI measurements are made to generate the restitution curve. Figure 2.4 shows beat number S1 and APD corresponding to stimuli S2 for varying PCL_{S2} values.

$$PCL = APD + DI \tag{2.4}$$

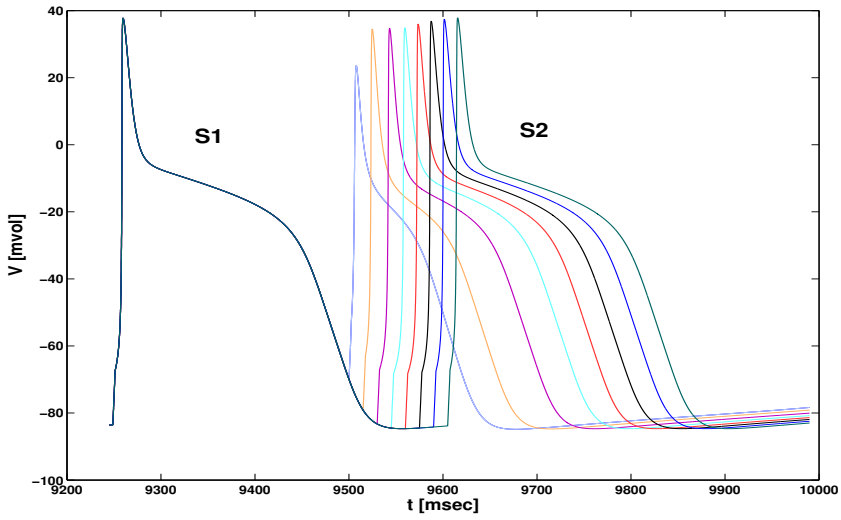

Figure 2.4: S1-S2 protocol.

As discussed in Sec.1.2, $[Ca^{2+}]$ is thought to be the inotropic state that is responsible for the force of contraction, indicating that alternation in the contractility is dependent on the concentration of Ca^{2+} ions. Lee et al. (Lab & Lee, 1990) in its experiments on isolated ferret ventricular muscle showed that alternations in contractility of a cardiac tissue is related to alternations in Ca^{2+}-*transient* peak concentrations (see Fig.2.5). Therefore, an alternation in voltage APD necessarily imply alternations in Ca^{2+} peak values. But unlike the voltage the Ca^{2+} is an intracellular concentration and does not diffuse or propagate though the cells along the cardiac tissue.

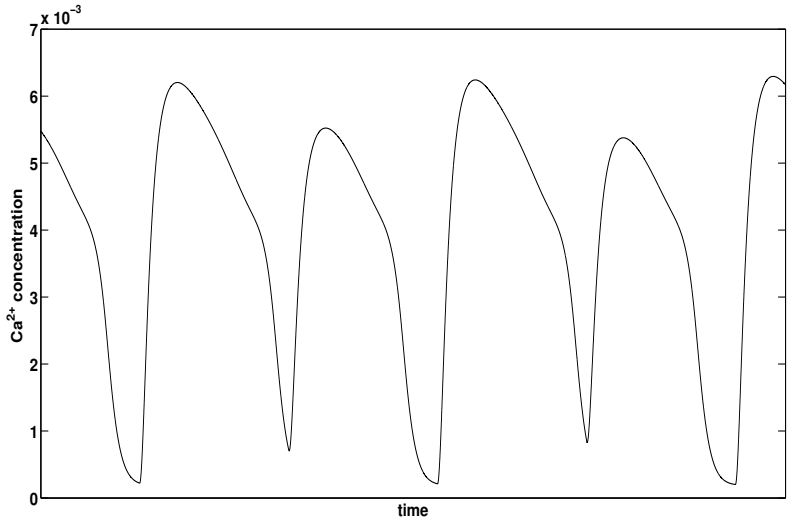

Figure 2.5: Time series plot showing alternations in Ca^{2+}-*transient* peak in LR1 model.

2.2.2 Control of Alternans in single cell

A single cardiac cell is reconstructed numerically using ionic currents suggested in LR1 model. The cell is paced faster than critical pacing interval (CPI) so as induce alternans (Fig.1.1). A control algorithm based on electrical pacing and the controlled pacing interval $T_{n(\xi=0)}$ is governed by the following equation:

$$T_n = \tau + (-1)^n \frac{\gamma}{2}(a_n) \tag{2.5}$$

where the pacing interval $\tau = 300$ for single cell, γ is the adjustable feedback gain for control of APD alternation at the pacing site, the amplitude of alternans, a_n is given as:

$$a_n = APD_n - APD_{n-1} \tag{2.6}$$

The value of feedback gain that can suppress alternans completely in a single cell is given as: (Echebarria & Karma, 2002)

$$1 - 1/f' < \gamma < 2/f' \tag{2.7}$$

where f' is the slope of the restitution curve. For LR1 model maximum slope is $f' = 2$ therefore, $0.5 < \gamma < 1$. For the purpose of simulations, value of γ was fixed at 0.6.

APD measurements are done at -50 mV i.e time is noted when during depolarization the voltage across the membrane crosses -50 mV in the upward direction and again during repolarization in the downward direction for the same voltage. Fig.2.6 shows the control of alternans in a single cell using the algorithm described as above. Beat numbers 1,2,3,4,5 and 6 clearly shows the development of alternans in a single cell. After beat number 6 a pacing controller described by Eq.2.5 is applied. The action of the controller to stabilize the alternans is shown by the beats following its initiation. The Cob-Web diagram in Fig.2.7 shows the stabilization of alternans due to the controller action. The solid-blue curve represents the nonlinear function $f(APD_n)$ that produces sustained alternans in a single cell. The hatched-red curve represents the manipulated function $f(APD, \tau + \delta\tau)$ which is due the action of controller (Eq.2.9). The controller action forces the system to move toward the point of intersection i.e. it successfully suppresses the alternans in the single cell for a given feedback gain γ.

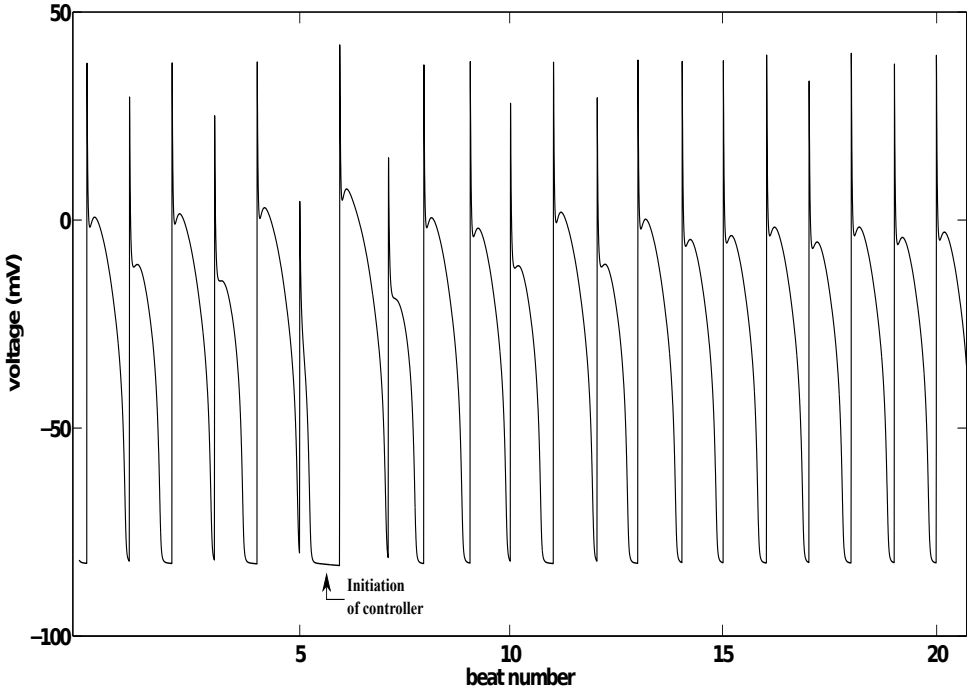

Figure 2.6: Control of alternans in single cell.

$$APD_{n+1} = f(APD_n, T_n) \tag{2.8}$$

T_n is defined as in Eq.2.5 and 2.6

$$APD_{n+1} = f(APD_n, \tau_n \pm \frac{\gamma}{2}(APD_n - APD_{n-1}))$$

$$APD_{n+1} = f(APD_n, \tau_n \pm \delta\tau) \tag{2.9}$$

$$where,\ \delta\tau = \frac{\gamma}{2}(APD_n - APD_{n-1}) \tag{2.10}$$

The fixed point in the system (APD^*, Y^*) has the property $APD^* = Y^*$,

$$\therefore\ APD_{n+1} = f(APD_n, \tau_n + \frac{\gamma}{2}(APD_n - Y_n)) \tag{2.11}$$

$$Y_{n+1} = APD_n \tag{2.12}$$

The Jacobian of this system is:

$$J = \begin{bmatrix} \frac{\partial f}{\partial APD_n} - \frac{\gamma}{2}\frac{\partial f}{\partial \tau} & \frac{\gamma}{2}\frac{\partial f}{\partial \tau} \\ 1 & 0 \end{bmatrix} \tag{2.13}$$

The fixed point is stable provided that J has eigenvalues which fall inside the unit circle. This condition is met for γ in the range given by Eq.2.7

2.2.3 Stabilization of Alternans in a one dimension cardiac tissue

In this section, we study the control of alternans in a 1D cable of length L = 6.25 cm. Luo-Rudy-1 (LR1) (Luo & Rudy, 1991) ionic currents are used to simulate the cardiac tissue numerically. LR1 is a mammalian ventricular cell based model which incorporates interaction between depolarization and repolarization and is a updated version of the Beeler-Reuter model (Beeler & Reuter, 1977) which also accounts for the calcium dynamics in cardiac myocyte. The 1D model of cardiac cell cable is given by the following nonlinear parabolic PDE as:

$$\frac{\partial V(\xi,t)}{\partial t} = D\frac{\partial^2 V(\xi,t)}{\partial \xi^2} - \frac{1}{Cm}I_{ion}(\xi,t) \tag{2.14}$$

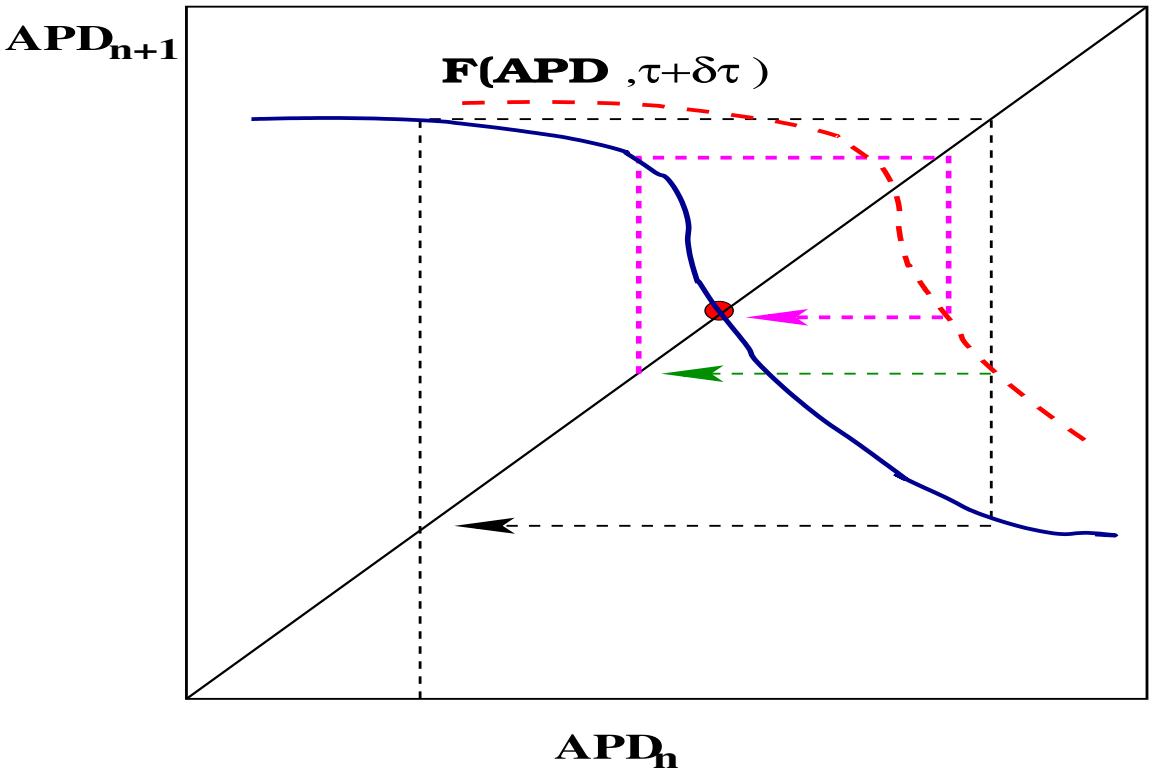

Figure 2.7: Cob-web diagram showing stabilization of alternans due to the action of controller.

Subject to boundary conditions,

$$\frac{\partial V(0,t)}{\partial \xi} = \frac{1}{C_m} I_{st}, \qquad \frac{\partial V(L,t)}{\partial \xi} = 0 \tag{2.15}$$

where, I_{st}/C_m refers to the electrical stimulus applied at L = 0.025cm i.e the first cell of the tissue. The constants, diffusion rate D = 1 X 10^{-3} cm^2/ms and membrane capacitance C_m = 1 $\mu F/cm^2$. The voltage evolution in the Eq.2.14 is calculated using finite difference approximation with mesh size $\Delta\xi = 0.025$. Standard explicit Euler integration scheme with step size $\Delta t = 0.05$ ms is applied. Due to the diffusive coupling term in Eq.2.14 this action potential propagates along length of the tissue away from the pacing site. In the simulations, APD is calculated between the voltage values $-50mV$. It is a well known fact that the cardiac tissue will manifest electrical alternans when the slope of the restitution curve is greater than unity at the critical pacing interval (CPI). This indicates that at lower DI, i.e at sufficiently short PCL the cardiac cell shall undergo alternans, which are manifested by an alternating pattern of long and short APDs. In a cardiac tissue two types of alternans can be observed 1) Concordant and 2) Discordant. When the alternans in the tissue are in same

phase then they are concordant in nature. These concordant alternans for shorter PCL, due to increased instabilities develop discordant alternans wherein the phase of alternans changes along the length of the tissue. The magnitude of instability also increases due the length of the tissue and may demonstrate discordant alternans directly at CPI. Fig.2.8 shows the discordant alternans in a cardiac tissue simulated as discussed above and paced at its CPI. The phase of alternans observed in Fig.2.8 is not the same along the tissue length, the tissue at the initial 1cm and towards the end show a short(S)-long(L)-short(S)-long(L) whereas middle section of tissue demonstrates an opposite pattern (L-S-L-S).

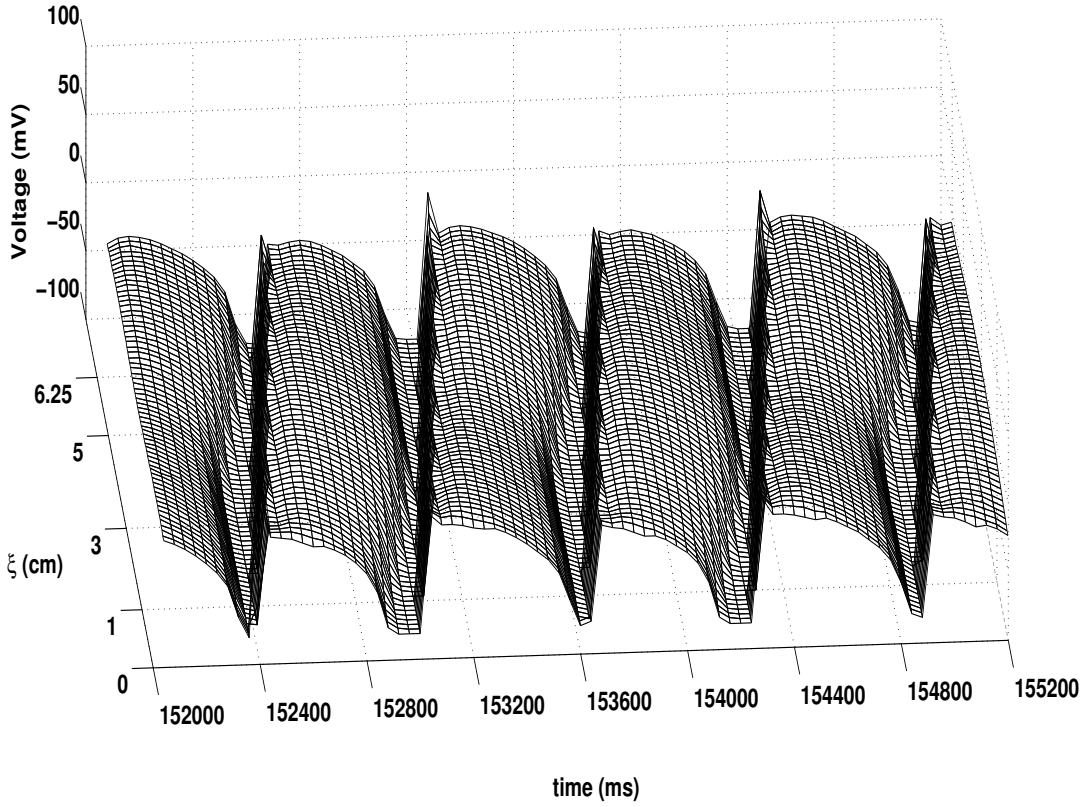

Figure 2.8: Transmembrane potential showing discordant alternans. A Long (L)-Short (S)-Long(L)-Short(S) pattern can be seen approximately between [0 1.5] cm and [4.5 6.25] cm whereas [1.5 4.5] cm of tissue shows S-L-S-L (discordant) pattern.

The amplitude of alternans , $a_n(\xi)$ for a 1D cardiac tissue is defined as:

$$a_n(\xi) = APD_n(\xi) - APD_{n-1}(\xi) \tag{2.16}$$

Stabilization of such alternans in a long cable can be achieved by coupling traditional

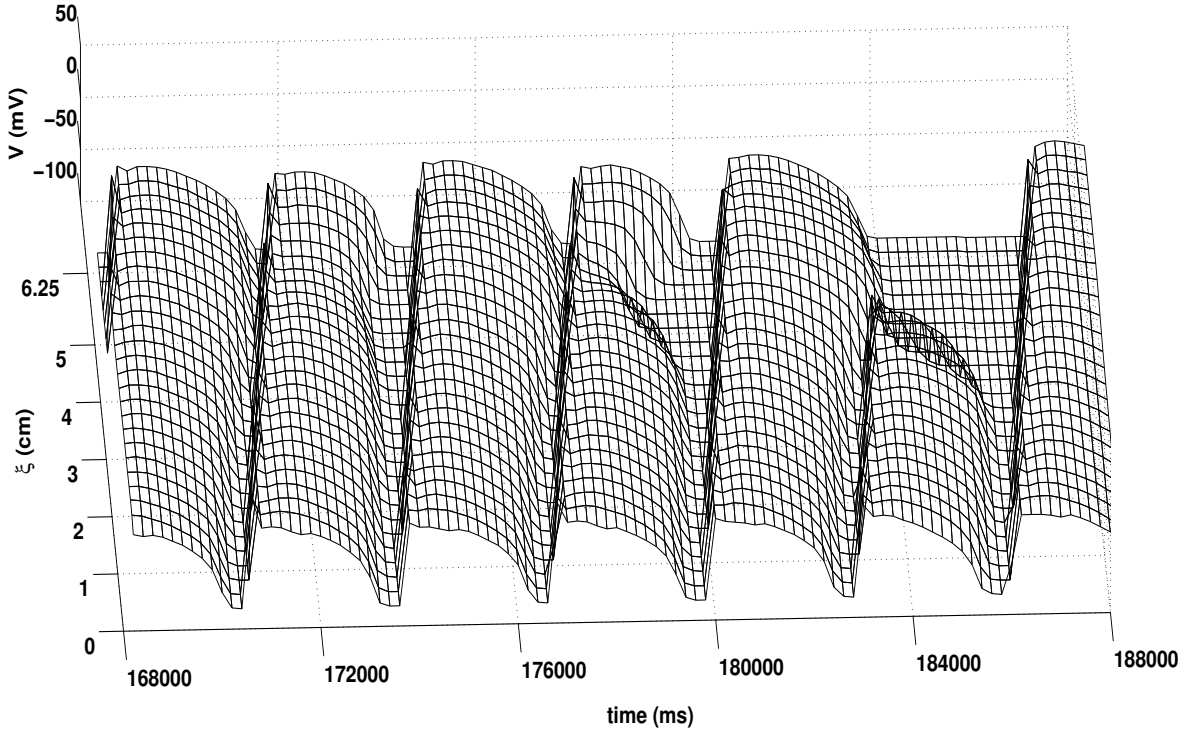

Figure 2.9: Transmembrane potential showing a conduction block.

electrical (at boundary) and spatially-distributed calcium feedback control. The boundary applied electrical feedback controller can be characterized as difference in APD values feedback at the pacing site similar to a pacing based controller in a single cell.

$$T_{n(\xi=0)} = \tau + \frac{\gamma}{2}(APD_{n(\xi=0)} - APD_{n-1(\xi=0)}) \tag{2.17}$$

where feedback gain is same as in single cell (γ = 0.6), τ = 311 ms, slightly higher than single cell. Previous works (Lin & Dubljevic, 2007, Dubljevic et al., 2008, Echebarria & Karma, 2002) have shown that simple feedback gain at the pacing site can effectively stabilize alternans only up to $\approx$ 1cm of length of tissue (see Fig.2.10). This limitation reduces the practical value of a controller based solely on gain based modulation of pacing interval. A pacing or electrical based boundary control successfully annihilates alternans up to $\approx$ 1cm but beyond that the instabilities grow along the length of the tissue and the tissue demonstrates concordant type of alternans but with higher amplitude which leads to a conduction block. To overcome this limitation of pacing based boundary control several such gain based pacing interval modulators can be placed multiple pacing sites but such a

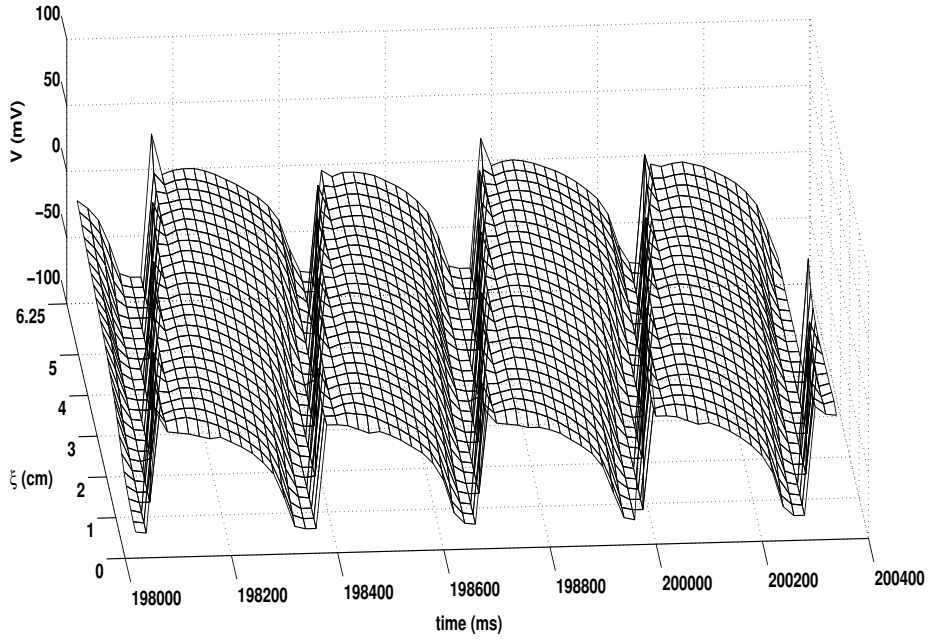

Figure 2.10: Schematic showing the transmembrane voltage(V) in a 1D tissue under electrical boundary based control. At the boundary no alternation in APD is seen whereas along the length alternation in APD increases.

control in a real heart adversely disrupts the normal voltage wave propagation across the tissue. Instead, modulation of intracellular calcium levels over a short length of tissue is used for the gain based spatially distributed control of alternans described by Eq 2.14. The calcium based spatially-distributed actuator is motivated by recent studies (Bers, 2001, Chudin et al., 1999, Kohl et al., 1999, Calaghan et al., 2003) which demonstrate that stretching of the cardiac myocyte modulates the internal calcium dynamics of the cell. Manipulating the calcium or mechanical properties of a cardiac cell affects the voltage APD (Calaghan et al., 2003). Hence, a controller is designed, that perturbs the mechanical properties or intracellular calcium in a cardiac cell so as to have a desirable effect on the APD to annihilate alternans The spatially distributed Ca^{2+}-controller acts after the electrical boundary feedback controller stabilizes a finite part of the cable ($\approx 1cm$). The spatially distributed Ca^{2+}-controller utilizes the difference between a stabilized delayed $[Ca]^{2+}$ at the pacing site and $[Ca]_i$ over the length of area under spatially-distributed control. The difference is used as input feedback correction term $[Ca]_{error}$ augmented with the cell calcium dynamics

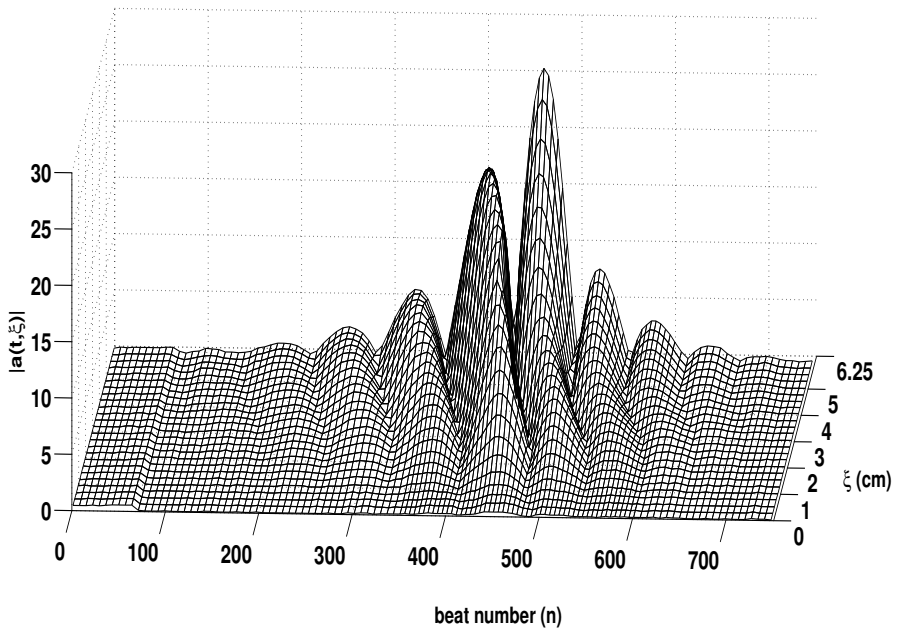

Figure 2.11: Time evolution of amplitude of alternans showing annihilation of alternans using a calcium based controller.

in the LR1 model.

$$[\dot{Ca^{2+}}]_i(t) = -10^{-4} I_{si} + 0.07(10^{-4} - [Ca]_i) + x[Ca^{2+}]_{err} \tag{2.18}$$

where the control action is restricted to,

$$x = \begin{cases} 0.03, & [\mathrm{Ca}^{2+}]_{err} < 0 \\ 0, & [\mathrm{Ca}^{2+}]_{err} \geq 0 \end{cases}$$

where $[\mathrm{Ca}]_{pacer}$, $[\mathrm{Ca}]_{i,control}$ are the intracellular calcium concentrations measured at the pacing site and sites under spatially-distributed control respectively. The gain x in Eq.2.18 is the amount of full state feedback applied as proportional control. τ_d is the time delay factor to account for the electrical wave propagation resistance along the cable length, i.e the measured $[\mathrm{Ca}]_{pacer}$ is compared with the $[\mathrm{Ca}]_{i,control}$ taking into consideration the time delay for the excitation of the i'th cell as compared to the excitation at the pacing site.

Control Algorithm with mixed boundary and spatially distributed calcium based controller

In the numerical study of the model described by Eq.2.14 and ionic currents from the LR1 model, we use the control protocol that couples electrical boundary control and spatially

distributed [Ca^{2+}]-control to stabilize a tissue of length over 1 cm without inducing conduction block (see Fig.2.9). A medically relevant size cardiac tissue of length L = 6.25 cm (a length necessarily greater than 1 cm) was considered. The tissue is initially paced at a sufficiently large pacing interval for approximately 10-15 beats and then suddenly dropped to a lower pacing interval such that there is no conduction block. The onsite pacing based controller applied at the boundary is initiated at approximately n = 40. The pacing interval for every beat is reduced by 1 ms until finally it drops τ= APD + DI = 307 ms, that induces sustained alternans with increasing amplitude which if not controlled leads to a conduction block. In order to suppress these alternans the previously discussed control strategy is employed to annihilate the instabilities. First electrical boundary pacing controller which is based on the difference in amplitude of two consecutive APDs is applied around beat number (n) $\approx$ 370. Applying such a control stabilizes the alternans along a finite length of the tissue ($\approx$ 1 cm) and the rest of the tissue manifests concordant alternans with an increasing amplitude (see Fig. 2.11). The spatially distributed Ca based controller is applied at n $\approx$ 450 over a region [3, 3.5] cm, the actuator compares the calcium concentration at the boundary $[Ca^{2+}]_{pacer}$ with the calcium concentration of the cell to be controlled ($[Ca^{2+}]_{i,control}$) and generates a control signal to compensate for the error. The error signal is attenuated by a proportional controller gain, x = 0.03. At a given pacing interval the Ca^{2+} transient peak is maximum in the alternans-free (or stabilized) cell. Therefore, the $Ca^{2+}{}_{pacer}$ peak concentration is higher than the Ca^{2+} that experiences alternans. In principle, the [Ca^{2+}]-controller is based on this difference in the stable and unstable Ca^{2+} concentrations. A spatially-distributed stabilizing [Ca^{2+}]-controller essentially operates only when the $[Ca^{2+}]_{err}$ is negative and its effect on calcium dynamics. The controller is active in the refractory phase of the APD that causes the Ca^{2+}-peak of the subsequent beat to increase. This necessarily drives the unstable (lower) Ca^{2+}-peak to an alternans free or stable peak value ($[Ca^{2+}]_{pacer}$). Such a combined electrical boundary pacing based and spatially distributed [Ca^{2+}] based controller could successfully annihilate the amplitude of alternans and avoid a conduction block coming from the non pacing end of the tissue.

Direct measurements of intracellular [Ca^{2+}] concentrations is difficult. Hence implementation of the spatially distributed controller can be carried out in two ways i) using the existing cardiac cell models to calculate the [Ca^{2+}] from local voltage (V) measurements

or ii) the controller can be based on a measurable quantity like mechanical deformations (stress) in the tissue. Therefore, in the next section a numerical study showing the effect of mechanical perturbations on cardiac alternans in a simple three variable Nash-Panfilov model is discussed.

2.3 The Amplitude Equation

In this section, we develop a analytical approach to annihilate the alternans in a cardiac tissue by applying the suggested control protocol. The spatiotemporal dynamics of small amplitude alternans associated with Eq. 2.14 in 1D paced cardiac tissue can be expressed in terms of the amplitude of alternans parabolic PDE developed by Echebarria and Karma (Echebarria & Karma, 2002). Further, this equation is coupled to include the spatiotemporal evolution of amplitudes of alternans associated with Ca^{2+} as suggested by Shiferaw and Karma (Shiferaw & Karma, 2006). A linear parabolic PDE exhibiting amplitude of alternans is given the following form:

$$\frac{\partial a(\xi,t)}{\partial t} = D\frac{\partial^2 a(\xi,t)}{\partial \xi^2} - w\frac{\partial a(\xi,t)}{\partial \xi} + \sigma a + \eta a_{Ca} \tag{2.19}$$

$$\frac{da_{Ca}(\xi,t)}{dt} = \gamma a(\xi,t) + \sum_{i=0}^{p} b_{Ca_i}(\xi) u_{Ca_i}(t)$$

Subject to boundary conditions:

$$\frac{\partial a(0,t)}{\partial \xi} = a(0,t) + u_b(t), \qquad \frac{\partial a(L,t)}{\partial \xi} = 0 \tag{2.20}$$

where $D = D_a/\tau$, $w = w/\tau$ and $\sigma = \sigma/\tau$, $D_a = \sqrt{d * APD_c}$ and $w = 2d/c$, d is the diffusion coefficient D given in Eq.2.14. In which APD_c is APD evaluated at the bifurcation point c is the propagation velocity along the length of the cable. The term $u_b(t)$ refers to boundary applied input associated with the electrical pacing based controller, while $\sum_{i=0}^{p} b_{Ca_i}(\xi) u_{Ca_i}(t)$ refers to spatially distributed calcium based controller, where $b_{Ca_i}(\xi - \xi_i) = \frac{1}{2\varepsilon} 1_{(\xi-\varepsilon,\xi_i+\varepsilon)}(\xi - \xi_i)$ represent the location of point and/or spatially uniform actuators placed within domain and p is associated with the number of actuators employed on the length of the cable. The dynamics of voltage alternans (a(ξ,t)), represented

by a PDE in Eq.2.19 are coupled with the calcium alternans ($a_{Ca}(\xi,t)$). The dynamics of calcium alternans are represented by an ordinary differential equation (ODE). In the expression for Ca^{2+} alternans the space (ξ) is a parameter as calcium alternans do not diffuse/propagate along the length of cable.

2.3.1 Identification of Amplitude Equation parameters

The amplitude equation parameters (σ, η and γ) are identified from ionic model (LR1) simulations in the following way.

- The identification of linear term σ is done by evaluating the logarithm of the slope of the restitution curve (refer Fig.2.2), period (τ_n) = APD_n+ DI_n. This *DI* is varied to get the restitution curve. This is done by the S1S2-protocol
  Measurements: DI_n, APD_{n+1}. $\sigma = \ln(f')$, where $APD_{n+1} = f(DI_n)$

- The factor γ, Shiferaw & Karma, 2006 signifies the dependence of $Ca^{2+}{}_{peak}$ concentration on DI (see Eq.2.19). A protocol similar to S1S2 is developed by which a relationship between changes in $Ca^{2+}{}_{peak}$ and DI (the rest time interval before S2) is established (Fig. 2.12). The minimum value for the slope of this curve is taken to be the value of γ.
  Measurements: transient- Ca^{2+} $peak_n$, transient- Ca^{2+} $peak_{n+1}$.

- For identification of η procedure similar to S1S2 is applied to produce a calcium signature. But in this case the S1 is the last beat in the series of approx 50 beats which are close to the bifurcation point just before the onset of alternans. Then S2 is generated by increasing the pacing period τ immediately after the S1. The calcium dynamics associated with this S2 beat is recorded as calcium signature. In a separate simulation run, the cell is paced for approx 50 beats at period near to the bifurcation point before onset of alternans. For the n+1 beat instead of natural cell calcium dynamics the calcium signature is used to impose the calcium dynamics (see Fig.2.13.a). η is given as the slope of the curve between APD and Δ Ca-peak (as shown in Fig.2.13.b).
  Measurements: APD_n, APD_{n+1}, transient- Ca^{2+} $peak_n$, transient- Ca^{2+} $peak_{n+1}$.

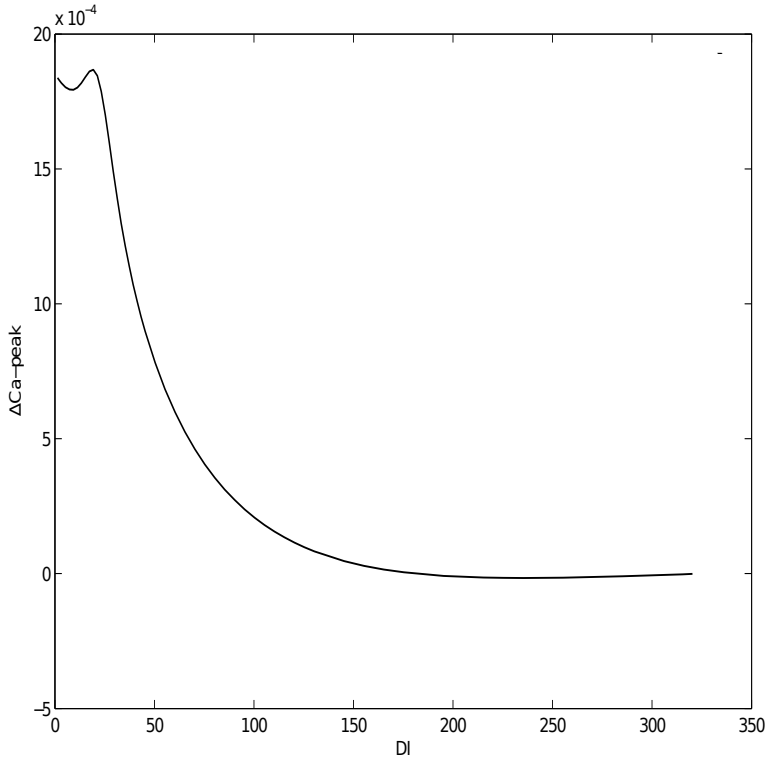

Figure 2.12: Effect of change in DI on Ca^{2+} peak.

2.3.2 Solution to the amplitude of alternans equation

An approximated delta function $\delta(\xi-\xi_0)=\frac{1}{2\varepsilon}1_{(\xi_0-\varepsilon,\xi_0+\varepsilon)}\in \mathcal{L}_2(0,L)$, is inserted into Eq.2.19. $\mathcal{L}_2(0,L)$ is a space of square integrable function on the domain [0,L]. Utilizing the approximated δ function, the boundary based input $u_b(t)$ in Eq.2.20 can be lifted to the amplitude of electrical alternans PDE to give,

$$\frac{\partial a(\xi,t)}{\partial t}=D\frac{\partial^2 a(\xi,t)}{\partial \xi^2}-w\frac{\partial a(\xi,t)}{\partial \xi}+\sigma a+\eta a_{Ca}+\delta(\xi)u_b(t) \tag{2.21}$$

$$\frac{da_{Ca}(\xi,t)}{dt}=\gamma a(\xi,t)+\sum_{i=0}^{p}b_i(z)u_{Ca}(t) \tag{2.22}$$

Subject to boundary conditions

$$\frac{\partial a(0,t)}{\partial \xi}=a(0,t),\qquad \frac{\partial a(L,t)}{\partial \xi}=0 \tag{2.23}$$

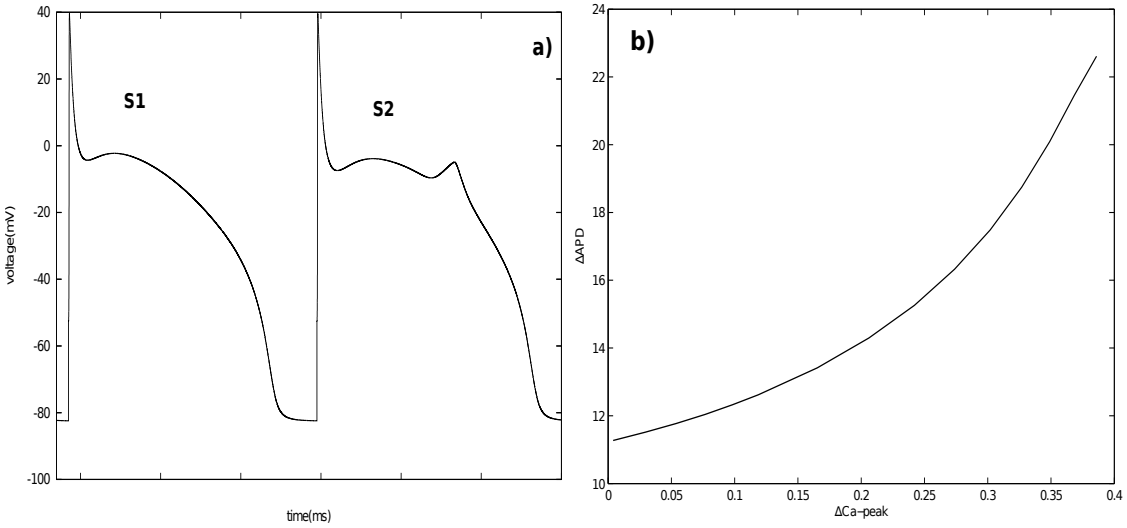

Figure 2.13: Determination of η a) Membrane potential showing change in action potential dynamics due to the sudden change in Ca^{2+} concentration, b) Effect of change in Ca^{2+} dynamics on APD.

This system of equations is amenable to modal decomposition. Thus let us assume solution to Eq.2.21 & Eq.2.22 is in the form:

$$a(\xi,t) = \sum_{n=1}^{\infty} a_n(t)\phi_n(\xi) \tag{2.24}$$

$$\sum_{i=0}^{p} b_{Ca_i} u_{Ca_i}(t) = \sum_{n=1}^{\infty} b_n(t)\phi_n(\xi) = \sum_{i=0}^{p} b_{Ca_i} u_{Ca_i}(t) \left[\sum_{n=1}^{\infty} b_n \phi_n(\xi) \right] \tag{2.25}$$

$$\delta(\xi) u_b(t) = \sum_{n=1}^{\infty} c_n(t)\phi_n(\xi) = u_b(t) \left[\sum_{n=1}^{\infty} c_n \phi_n(\xi) \right] \tag{2.26}$$

implies that

$$\sum_{n=1}^{\infty} b_n(t)\phi_n(\xi) = \sum_{i=1}^{p} b_{Ca_i} \qquad \sum_{n=1}^{\infty} c_n(t)\phi_n(\xi) = \delta(\xi) \tag{2.27}$$

A linear operator $\mathcal{A}$ can be defined as,

$$\mathcal{A}\phi(\xi) = (D\frac{\partial^2}{\partial \xi^2} - w\frac{\partial}{\partial \xi} + \sigma)\phi(\xi)$$

Applying a separation variables method around the spatially uniform unstable steady-state $a(\xi,t) = 0$, one obtains the operator $\mathcal{A}$ which belongs to the class of Sturm-Liouville

operators,

$$\mathcal{A}\phi_n(\xi) = \left(D\frac{\partial^2}{\partial \xi^2} - w\frac{\partial}{\partial \xi} + \sigma \right) \phi_n(\xi) = \lambda_n \phi_n(\xi) \tag{2.28}$$

Subject to

$$\frac{d\phi_n(0)}{d\xi} = \phi_n(0), \qquad \frac{d\phi_n(L)}{d\xi} = 0 \tag{2.29}$$

Multipling Eq.2.28 by $\frac{1}{D}e^{-w\xi/D}$ and rearranging terms

$$De^{w\xi/D}\frac{d}{d\xi}\left(e^{-w\xi/D}\frac{d\phi_n}{d\xi} \right) + (\sigma - \lambda_n)\phi_n(\xi) = 0 \tag{2.30}$$

Comparing with the Strum-Liouville form:

$$L(.) = \frac{1}{\rho(\xi)}\frac{d}{d\xi}(p(\xi)\frac{d(.)}{d\xi}) + q(\xi)(.) = 0 \tag{2.31}$$

we get,

$$\begin{aligned} \rho(\xi) =& \frac{1}{D}e^{-w\xi/D} \\ p(\xi) =& e^{-w\xi/D} \\ q(\xi) =& (\sigma - \lambda_n) \end{aligned} \tag{2.32}$$

Thus, $\phi_n(\xi)$ is the system of eigenfunction and $\phi_n^*(\xi) = \frac{1}{D}e^{-w\xi/D}\phi_n(\xi)$ is the adjoint eigenfunction. The above Sturm-Louville problem can be simplified to the following transcendental equation:

$$\tan(\sqrt{\beta_n}L) = \frac{\sqrt{\beta_n}}{\beta_n - \frac{w}{2D}\left(1 - \frac{w}{2D}\right)} \tag{2.33}$$

where β_n is the solution to the above transcendental equation and the spectrum of eigenvalues of operator $\mathcal{A}$ are given as (see Fig.2.14),

$$\lambda_n = \sigma - \left(\beta_n + \frac{w^2}{4D^2} \right) \tag{2.34}$$

In terms of the system eigenfunctions, the solution to Eq.2.34 is:

$$\phi_n(\xi) = B_n e^{w\xi/2D}\left[cos\left(\sqrt{\beta_n}\xi \right) + \left(1 - \frac{w}{2D} \right)\frac{1}{\sqrt{\beta_n}} sin\left(\sqrt{\beta_n}\xi \right) \right] \tag{2.35}$$

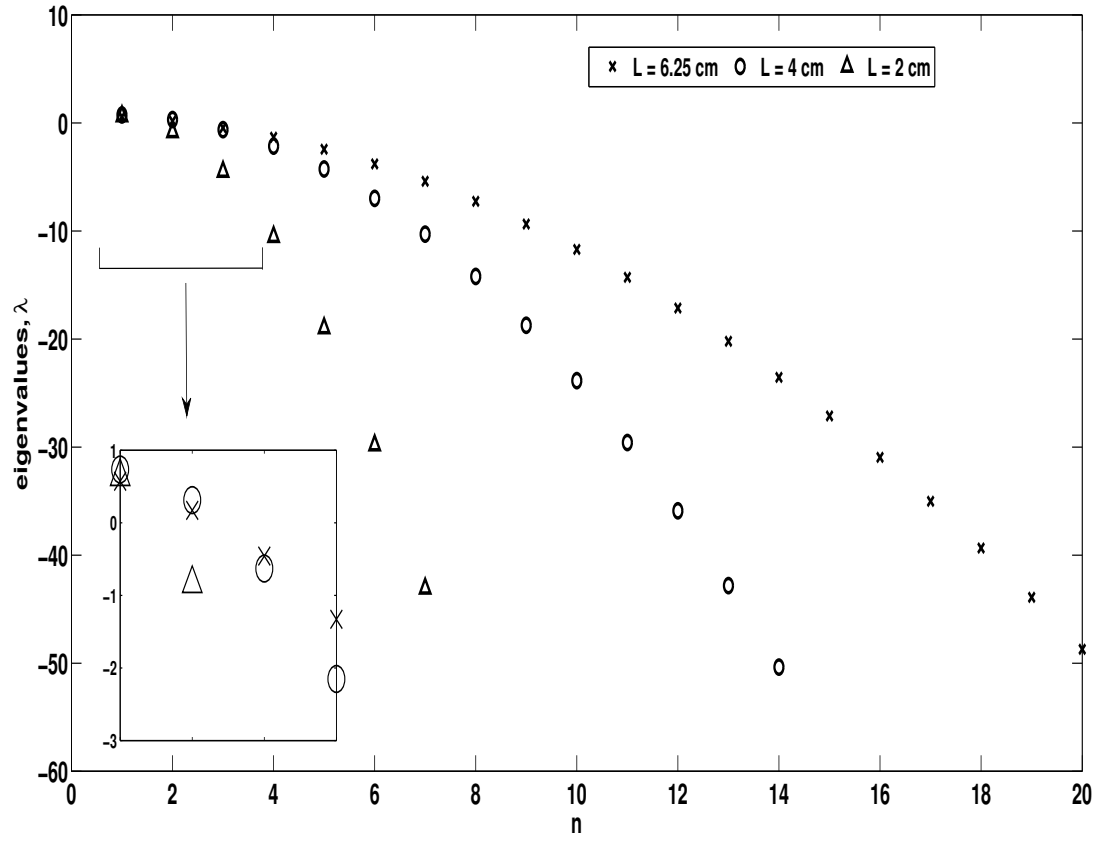

Figure 2.14: Spectrum of eigenvalues determined by for cable lengths (2 cm, 4 cm, 6.25 cm).

where B_n is chosen to make the eigenfunctions orthonormal to the adjoint eigenfunctions, given as:

$$B_n = \left[\int_0^L \left(cos\left(\sqrt{\beta_n}\xi\right) + \left(1 - \frac{w}{2D}\right) \frac{1}{\sqrt{\beta_n}} sin\left(\sqrt{\beta_n}\xi\right) \right)^2 d\xi \right]^{-\frac{1}{2}} \tag{2.36}$$

Finally, the modal form is obtained by projecting Eq.2.21 on the space of eigenfunction of operator $\mathcal{A}$ though Galerkin's method to yield:

$$\frac{da_n}{dt} = \lambda a_n + \eta a_{Ca_n} + \phi_n(0) u_b(t) \tag{2.37}$$

$$\frac{da_{Ca_n}}{dt} = \gamma a_n + \sum_{i=0}^{p} < b_i(\xi), \phi_n > u_{Ca_i}(t) \tag{2.38}$$

Thus we have accomplished the exact modal decomposition, where the lumped system

equations are given by Eqs.2.37 -2.38 which can be directly used in a control synthesis scheme. The coefficients b_n and c_n are given from the orthogonality relations:

$$b_n = \int_0^L b_{Ca_i}(\xi)\phi_n d\xi = < b_{Ca_i}(\xi), \phi_n > \qquad n = 1,2,3,... \tag{2.39}$$

$$c_n = \phi_n(0) = B_n \qquad n = 1,2,3,... \tag{2.40}$$

The output of the system given by Eqs.2.37 - 2.38 is given as:

$$Y = \begin{bmatrix} < C(\xi)a(\xi,t), \phi_n > \\ \\ < C(\xi)a_{Ca}(\xi,t), \phi_n > \end{bmatrix} \tag{2.41}$$

$$Y = \begin{bmatrix} \int_0^L \sum_{n=1}^{\infty} a_n(t)\phi_n(\xi)C(\xi)\phi_j d\xi & 0 \\ 0 & \int_0^L \sum_{n=1}^{\infty} a_{Ca_n}(t)\phi_n(\xi)C(\xi)\phi_j d\xi \end{bmatrix} \tag{2.42}$$

Considering that states a(ξ,t)$_n$ and a(ξ,t)$_{Ca_n}$ are fully measurable, hence C(ξ) = 1 and:

$$\int_0^L \phi_n(\xi)\phi_j d\xi = \begin{cases} 1, & \text{if, j = n} \\ 0, & \text{else} \end{cases}$$

Therefore, Eqs.2.37 - 2.38 can be represented in state space form as:

$$\begin{bmatrix} \dot{a_n} \\ \dot{a}_{Ca_n} \end{bmatrix} = \begin{bmatrix} \lambda_n & \eta_n \\ \gamma_n & 0 \end{bmatrix} \begin{bmatrix} a_n \\ a_{Ca_n} \end{bmatrix} + \begin{bmatrix} \phi_n(0) & 0 \\ 0 & < b_{Ca_i}(\xi), \phi_n > \end{bmatrix} \begin{bmatrix} u_b(t) \\ u_{Ca}(t) \end{bmatrix}$$

$$Y = \begin{bmatrix} 1 & 0 \\ 0 & 1 \end{bmatrix} \begin{bmatrix} a_n \\ a_{Ca_n} \end{bmatrix} \tag{2.43}$$

so that, finally the A,B,C triplet is given by:

$$A = \begin{bmatrix} \lambda_n & \eta_n \\ \gamma_n & 0 \end{bmatrix}, B = \begin{bmatrix} \phi_n(0) & 0 \\ 0 & < b_{Ca_i}(\xi), \phi_n > \end{bmatrix}$$

$$C = \begin{bmatrix} 1 & 0 \\ 0 & 1 \end{bmatrix}$$

where, n is the number of modes considered (or the number of eigenfunctions in Galerkin's method used to numerically simulate the system)

2.4 Controller synthesis

A state feedback control is applied on the state space model described in Eq.2.43. Simulations were carried out in MATLAB. For a cable of length $L = 6.25cm$ the operator $\mathcal{A}$ has

two unstable modes and calcium amplitude equation has two unstable modes. The stability analysis shows that these four eigen modes are stabilizable and hence the complete system can be stabilized. The eigenvalues of stable modes remain invariant under the state feedback control structure.

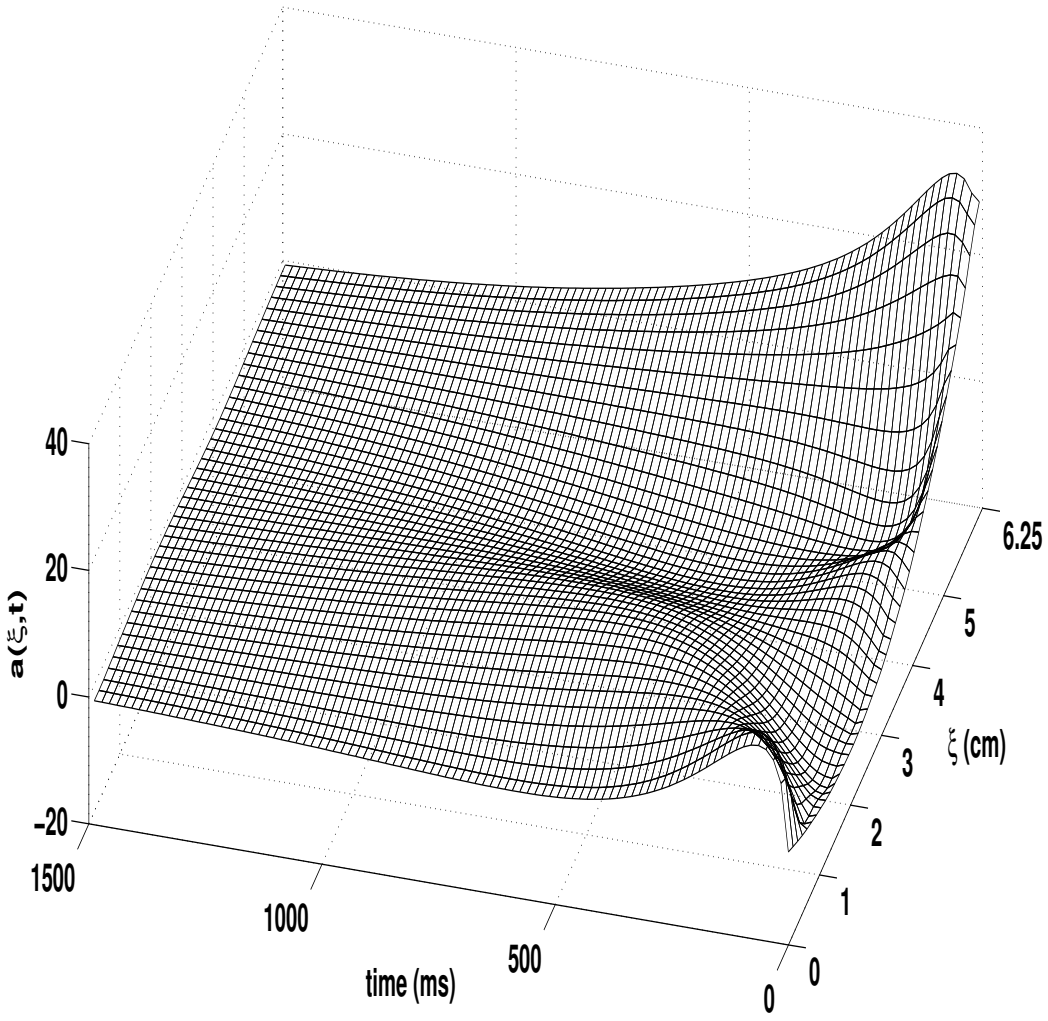

Figure 2.15: Boundary and spatially distributed Ca^{2+} control of instabilities given by Eq.2.14: Stabilization of voltage alternans.

Input to the system is given as a full state feed back, $U(t) = -kX(t)$, where

$$U(t) = \begin{bmatrix} u_{Ca}(t) & u_b(t) \end{bmatrix} \quad , X(t) = \begin{bmatrix} a_n \\ a_{Ca_n} \end{bmatrix}$$

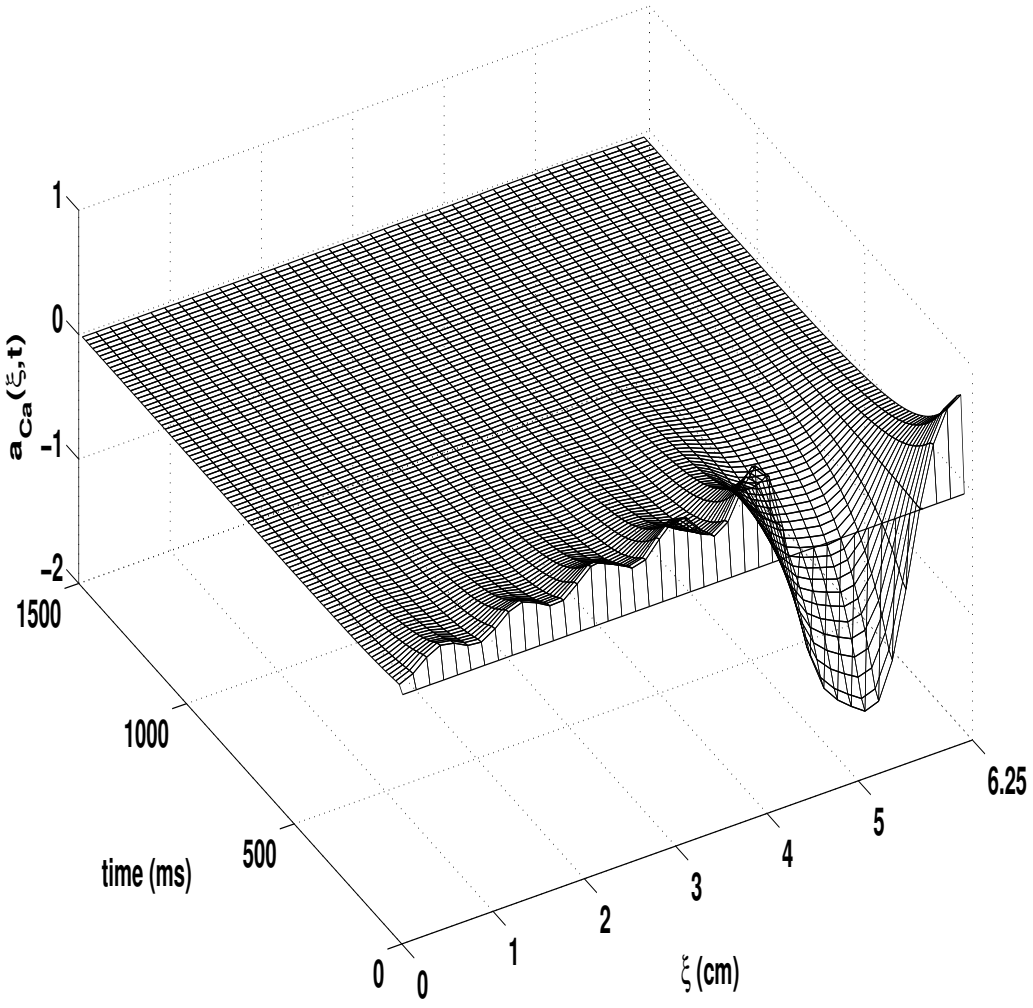

Figure 2.16: Boundary and spatially distributed Ca^{2+} control of instabilities given by Eq.2.14: Stabilization of Ca^{2+} alternans.

and k is the gain matrix such that u_b is the electrical boundary applied feedback controller as discussed in Section.2.3 that can stabilize only a finite range of cable length($\approx 1cm$). To annihilate the alternans along the full length of the cable, a spatially distributed Ca^{2+}-controller is applied which compares the calcium concentration of the cells under control with the calcium concentration at the boundary and generates an equivalent control signal. Such spatially distributed Ca^{2+}-controller actuators are placed at ξ_i between $\xi = 4.375cm$ and $\xi = 5.625cm$.

Usual pole placement or optimal control techniques can be applied to stabilize the above system. Prior to such control techniques the system model can be reduced to a state space realization that isolates the stable part of the system matrix and control can be applied to only the unstable eigenvalues. In MATLAB, command *balreal*[*] was used to determine a state transition matrix that yields the following state- space realization of the model described in Eq.2.43.

$$\begin{bmatrix} \dot{X} \end{bmatrix} = \begin{bmatrix} A_{unstable} & 0 \\ 0 & A_{stable} \end{bmatrix} \begin{bmatrix} X \end{bmatrix} + \begin{bmatrix} B_{unstable} \\ B_{stable} \end{bmatrix} \begin{bmatrix} U(t) \end{bmatrix}$$

$$Y = \begin{bmatrix} C_{unstable} & C_{stable} \end{bmatrix} X \tag{2.44}$$

where,

$$X = \begin{bmatrix} a \\ a_{Ca} \end{bmatrix}$$

With this state space model and only the unstable eigenvalues to stabilize the *care*[†] command in MATLAB is used to determine the unique stabilizing optimal controller-gain k. Both voltage and calcium profiles show stabilization of the instability caused by alternans given by Eq.2.14 with the application control protocol (see Fig.2.15 and Fig.2.16). A comparative study of stabilization of alternans by 1) only electrical boundary based control only and 2) boundary control with spatially distributed calcium control shows that amplitude of boundary controller gain required in the latter case is much smaller and less oscillatory nature and hence have a higher possibility of application in a human heart tissue(see Fig.2.17).

This analysis of linear parabolic PDE reveals that stabilization of alternans is possible with a control structure that is realizable in a real heart tissue. Also the results obtained from this model are in close agreement with those from the ionic model.

[*]Computes a balanced realization for the stable portion of the LTI model for both continuous and discrete systems. In MATLAB, *[sysb, g] = balreal(sys)*, returns a state space realization *sysb* consisting of stable modes. For stable systems, *sysb* is an equivalent realization for which the controllability and observability gramians are equal and diagonal, their diagonal entries forming the vector G of Hankel singular values. Small entries in G indicate states that can be removed to simplify the model. If *sys* has unstable poles, its stable part is isolated, balanced, and added back to its unstable part to form sysb. The entries of *g* corresponding to unstable modes are set to *Inf*

[†]computes the unique solution of the continuous-time algebraic Riccati equation

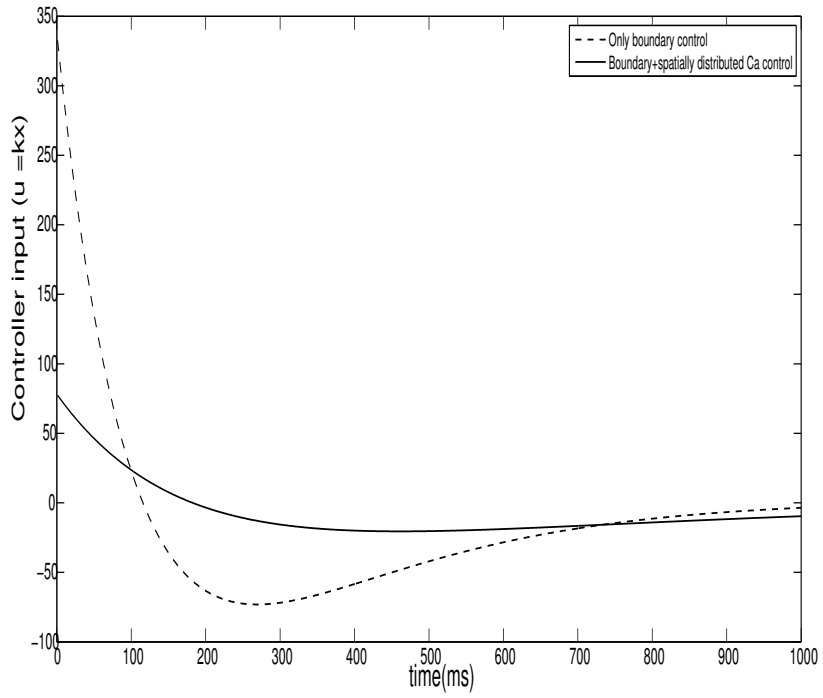

Figure 2.17: Amplitude of feedback boundary based pacing input signal in case of only boundary control and boundary control with spatially distributed Ca control.

Chapter 3

Mechano-Electric Feedback

3.1 Introduction to Electromechanical cardiac cell model

It is known that electric activity in the heart affects the mechanical properties of the heart. The sudden rise in electric potential (depolarization) induces a cardiac cell to undergo mechanical contraction and relaxation during the diastolic interval (see Fig.3.1). This mechanical activity of the cardiac cell is attributed to the release of Ca^{2+} ions due to electric potential and their binding and unbinding with contractile proteins, mainly Troponin C. This effect of electrical activity on mechanical properties of a cardiac cell is termed as the excitation-contraction coupling. Studies have also indicated that any manipulation in the mechanical stress of cardiac cell subsequently affects the electrical properties of the tissue. Experiments carried out Calaghan et al. (Calaghan et al., 2003) on guinea pig ventricular myocytes concluded that a mechanical stretch in the direction of the fibre increased the action potential duration (APD). Models described in Sec.2.1 do not take into consideration this electrical and mechanical stress-strain relationship of a cardiac cell. The heart cells usually contract to approx. 15-20% of their original length. To account for such high deformations, stress-strain dynamics are based on finite deformation elasticity theory. In literature various models (Nash & Panfilov, 2004, Niederer et al., 2006) describing the electro-mechanical coupling are available. The purpose of this chapter is to validate the suggested controller algorithm by showing that a mechanical based perturbation can affect the electrical properties of a cardiac tissue and also stabilize alternans in the tissue.

The Nash-Panfilov model (Nash & Panfilov, 2004) is a simple three variable FitzHugh-Nagumo (FHN) type model coupled with mechanical stress-strain properties for a cardiac

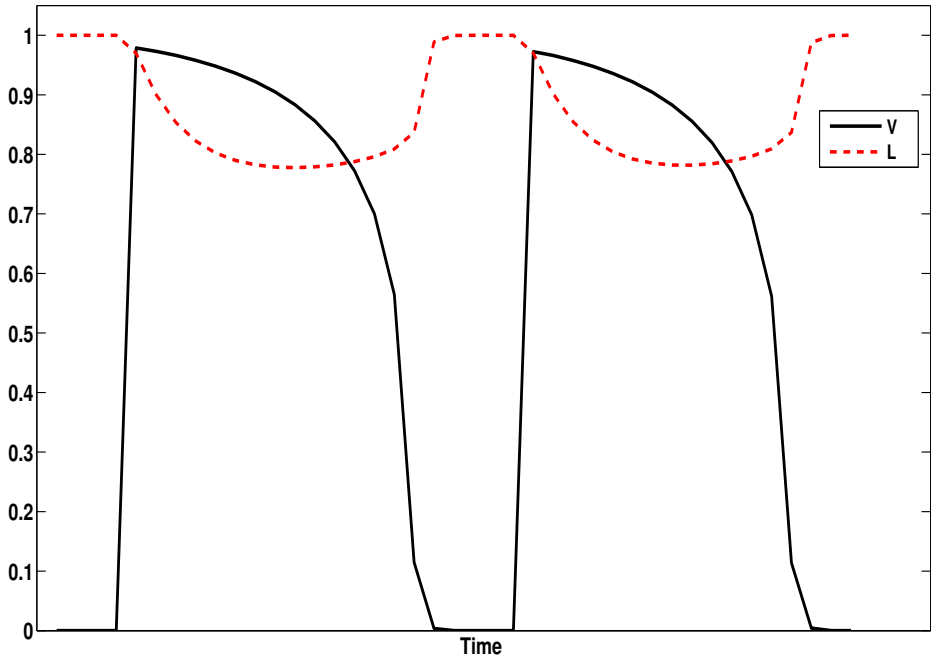

Figure 3.1: Dependence of mechanical properties (length, L) on the electrical activity (voltage, V) in a single cell (Voltage and Length are dimensionless).

cell. The Nash-Panfilov (NP) model includes an additional third variable to the Aliev-Panfilov model (Aliev & Panfilov, 1996) which is associated with the active tension in the cell. This active tension which is a function of the electrical voltage in the tissue is further linked to the mechanics model. The purpose of this chapter is just to study and annihilate alternans via mechanical perturbations for which the exact shape of the action potential is not necessary. Newly develop ionic models can reconstruct the action potential that is equivalent to a realistic cardiac cell that are computationally complex and expensive. As this part of the thesis neither requires an exact action potential shape nor description of any chemical species a simple NP model is used to numerically reconstruct a cardiac cell dynamics.

3.2 Cardiac tissue mechanics model

The cardiac tissue mechanical analysis is based on the the finite elastic deformation theory. The finite deformation gradient tensor, **F** that transforms the undeformed cell geometry to

a deformed is given as:

$$F_M^i = \frac{\partial x_i}{\partial X_m}, \tag{3.1}$$
$$\mathbf{F} = \frac{\partial \mathbf{x}}{\partial \mathbf{X}}$$

where x_i denote the deformed position of the particle, X_M denote the reference (undeformed) material coordinates and i,M = 1,2,3. Therefore, **F** denotes a map that transforms a material line segment from a undeformed geometry d**X** to a deformed geometry d**x**.

The Cauchy-Green deformation tensor **C** and Langrange-Green strain tensor **E** are defined as

$$\mathbf{C} = \mathbf{F}^T\mathbf{F}, \tag{3.2}$$
$$\mathbf{E} = \frac{1}{2}(\mathbf{C} - \mathbf{I}), \tag{3.3}$$

where I is the identity matrix.

The equilibrium conditions arise from the conservation of linear momentum following Newtons's laws of motion. For static equilibrium in the absence of body forces, the governing equations expressed in terms of second Piola-Kirchhoff stress components,

$$\frac{\partial}{\partial X_m}(T_{MN}F_N^i) = 0, \tag{3.4}$$
$$\frac{\partial}{\partial X_m}(S_{MN}) = 0, \tag{3.5}$$
$$M,N = 1,2,3$$

where S_{MN} is the first Piola-Kirchoff stress tensor and T_{MN} is the second order Piola-Kirchoff stress tensor given as:

$$T_{MN} = T_{MN}^{passive} + T_{MN}^{active} \tag{3.6}$$

The component T_{MN}^{active} has components that are obtained from the electrophysiological model and is responsible to for mechanical deformations. The individual components of

$T_{MN}^{passive}$ and T_{MN}^{active} are given as:

$$T_{MN}^{passive} = T^W - p(C_{MN}) \tag{3.7}$$

$$T^W = \frac{1}{2}\left(\frac{\partial W}{\partial E_{MN}} + \frac{\partial W}{\partial E_{NM}}\right) \tag{3.8}$$

$$T_{MN}^{passive} = \frac{1}{2}\left(\frac{\partial W}{\partial E_{MN}} + \frac{\partial W}{\partial E_{NM}}\right) - p(C_{MN}) \tag{3.9}$$

$$T_{MN}^{active} = T_a C_{MN} \tag{3.10}$$

where $E_{NM} = (E_{MN})^T$, $C_{MN} = (C^{MN})^{-1}$, W is the strain energy function defined as

$$W = c_1(I_1 - 3) + c_2(I_3 - 3) \tag{3.11}$$

$$I_1 = tr\mathbf{C},\ I_2 = \frac{1}{2}[(tr\mathbf{C})^2 - tr\mathbf{C}^2],\ I_3 = det\mathbf{C}$$

I_1, I_2 and I_3 are the principal invariants of Cauchy-Green stress tensor, **C**, and $tr\mathbf{C}$ is trace of **C** given by the sum of principal diagonal elements.

3.3 Numerical Simulations using Nash-Panfilov (NP) model

Equations governing the electrophysiological parameters of NP model in one dimension are described as follows:

$$C_m\frac{\partial V}{\partial t} = D\frac{\partial}{\partial X_i}(\sqrt{C}C^{MN}\frac{\partial V}{\partial X_i}) - f(V) \tag{3.12}$$

$$\frac{\partial r}{\partial t} = (\varepsilon + \frac{\mu_1}{\mu_2 + V})(-r - kV(V - a - 1)) \tag{3.13}$$

$$\frac{\partial T_a}{\partial t} = \varepsilon(V)(k_{Ta}V - T_a) \tag{3.14}$$

$$\frac{\partial}{\partial t}(S^{MN}) = 0 \tag{3.15}$$

where $f(V) = kV(V-1)(V-a) - rV - I_g$, V is dimensionless transmembrane potential, r is the recovery variable, T_a is the active stress and D is the diffusion constant. The electrophysiological model described by Eqs.3.12 - 3.14 coupled with the cardiac mechanics described by Eqs.3.1 - 3.11 together form the NP model. The term $\mathbf{F(X)} = \partial\mathbf{x}/\partial\mathbf{X}$ introduces non linearity in the system and requires rigorous numerical techniques to ensure the stability. Hence, a linear approximation for **F(X)** is done and the model is simulated

as a coupled system (Alvarez-Lacalle & Echebarria, 2009). With T^W as in Eq.3.9) the mechanics equations for 1D can be reduces to

$$T^W = 2c_1 I \tag{3.16}$$

$$S^W = T^W.F(X)$$

$$\therefore\ S^W = 2c1.F(X) \tag{3.17}$$

$$S^{passive} = S^W + pdet(F)\mathbf{F}^{-1} \tag{3.18}$$

The last term in Eq.3.18 maintains the isotropic conditions which is non zero in absence of external forces also for incompressible materials $det(\mathbf{F}) = 1$. From initial conditions when $\mathbf{F} = 1$ and forcing $S^{passive} = 0$ gives $p = 2c_1 = \tilde{c}$. Hence, total $S = S^{passive} + S^{active}$

$$S = S^W - \tilde{c}\,\mathbf{F}^{-1} + T_a\mathbf{C}^{-1}\mathbf{F} \tag{3.19}$$

from Eq.3.15

$$\frac{\partial}{\partial X}\left[S^W - \tilde{c}\,\mathbf{F}^{-1} + \frac{T_a(X)}{F(X)}\right] = 0$$

$$\frac{\partial}{\partial X}\left[\tilde{c}\,\mathbf{F} - \tilde{c}\,\mathbf{F}^{-1} + \frac{T_a(X)}{F(X)}\right] = 0 \tag{3.20}$$

Eq.3.20 when considered without the constant pressure term is given as:

$$\frac{\partial}{\partial X}\left[\tilde{c}\,\mathbf{F} + \frac{T_a(X)}{F(X)}\right] = 0 \tag{3.21}$$

Eq.3.21 when integrated and linear deformation approximation for deformation gradient, $\mathbf{F(X)} = 1 + u(X)$ with $u \ll 1$, gives:

$$\tilde{c}[1 + u(X)] + T_a(X)[1 - u(X)] = A \tag{3.22}$$

$$F(X) = 1 + u(X) = \frac{(A - T_a(X))}{\tilde{c}}$$

where A is a constant of integration to be determined. Using the boundary conditions [$x(0) = 0$ and $x(L) = L$] yields

$$\int_0^L F(X)dX = L \tag{3.23}$$

$$\therefore\ A = \tilde{c} + \bar{T}_a,\ \bar{T}_a = avg(T_a(X))$$

$$F(X) = 1 + \frac{(\bar{T}_a - T_a(X))}{\bar{c}} \tag{3.24}$$

At any particular position when $\bar{T}_a > T_a$ signifies that the tissue undergoes elongation or stretch. Current I_g described in Eq (3.12) is active only when the cell stretches locally and it is given as, $I_g = (g/\bar{c})(V-1)(\bar{T}_a - T_a)^2$. For the purpose of numerical simulations, Eq.3.12-Eq.3.15 are used to constitute the electromechanical model and Eq.3.24 gives the mechanical deformation gradient. A one dimension cable of length $L = 7\,cm$ is considered. Eq.3.1 is evaluated numerically by semi implicit finite difference method as time integration scheme with Δt = 0.02 and $\Delta X = 0.1$. The tissue is paced at the boundary to its critical pacing length (PL) such that the APD alternates (Fig.3.2).

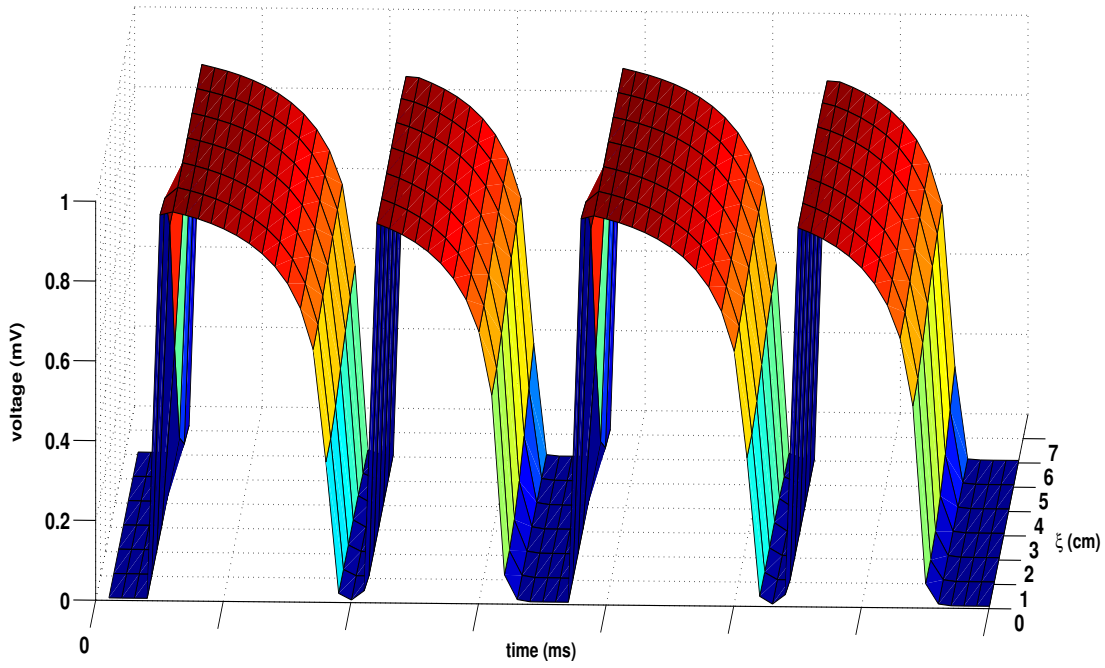

Figure 3.2: Concordant alternans in APD in Nash-Panfilov model.

APD measurements are done when voltage crosses 0.4 units. Amplitude of alternans is given by the difference between two APDs.

$$a_n(\xi) = APD_n - APD_{n-1} \tag{3.25}$$

Under constant critical PL the amplitude of alternans grows (see Fig.3.3) finally ending into a conduction block (not shown here). A spatially distributed mechanical based perturbations are carried out on the tissue to annihilate alternans. Basic full state feedback

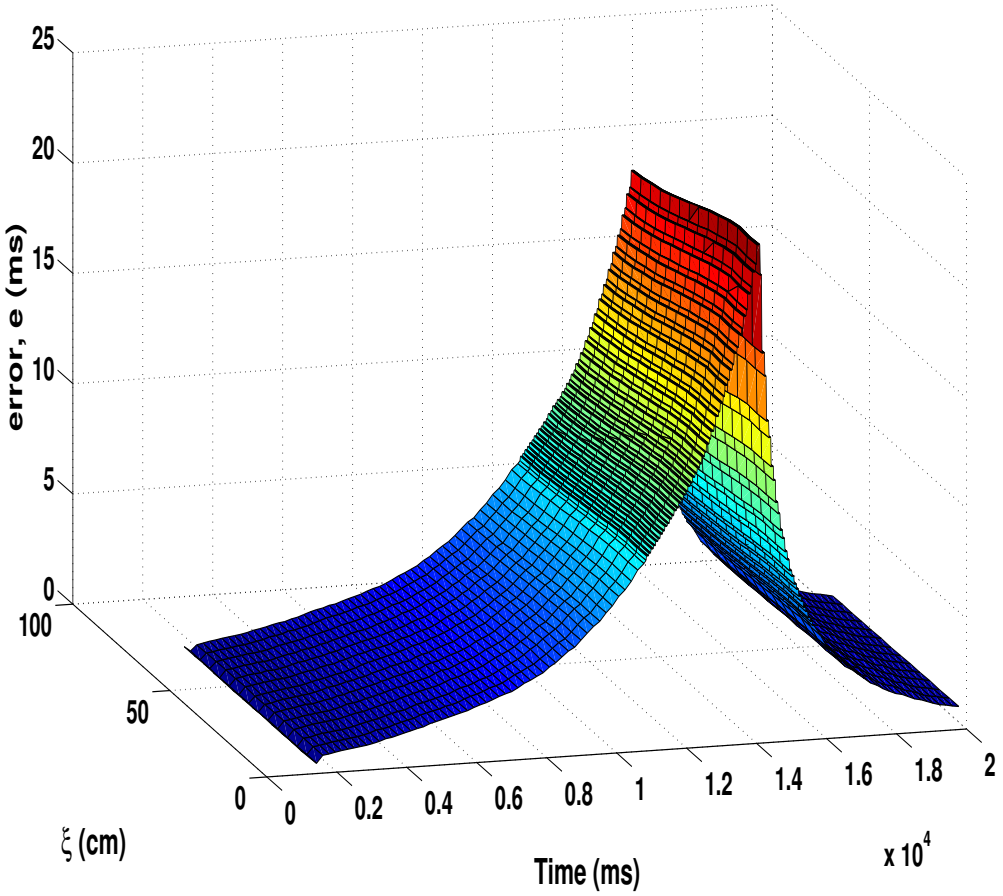

Figure 3.3: Amplitude of alternans - Nash Panfilov (NP) model.

algorithm which takes error e (see Eq.3.26) generated between two consequent APDs provides a control signal which is applied over the region 3-4.5 cm. The control signal is active only when $e < 0$ due to which the controller only acts on the long-APD (see Fig.3.4 after 14000 ms, when the controller is activated) . Thus, Eq(3.14) is modified to incorporate the spatially distributed controller by adding an error based controller that perturbs the active tension in the cells, given as:

$$e = (APD_n - APD_{n-1}) \tag{3.26}$$

$$\partial_t T_a = \varepsilon(V)(k_{Ta}V - T_a) + \beta e \tag{3.27}$$

From Fig.3.3 we see that the alternans developed in the cardiac tissue can be annihilated by using a spatially distributed mechanical stress-strain based controller which was

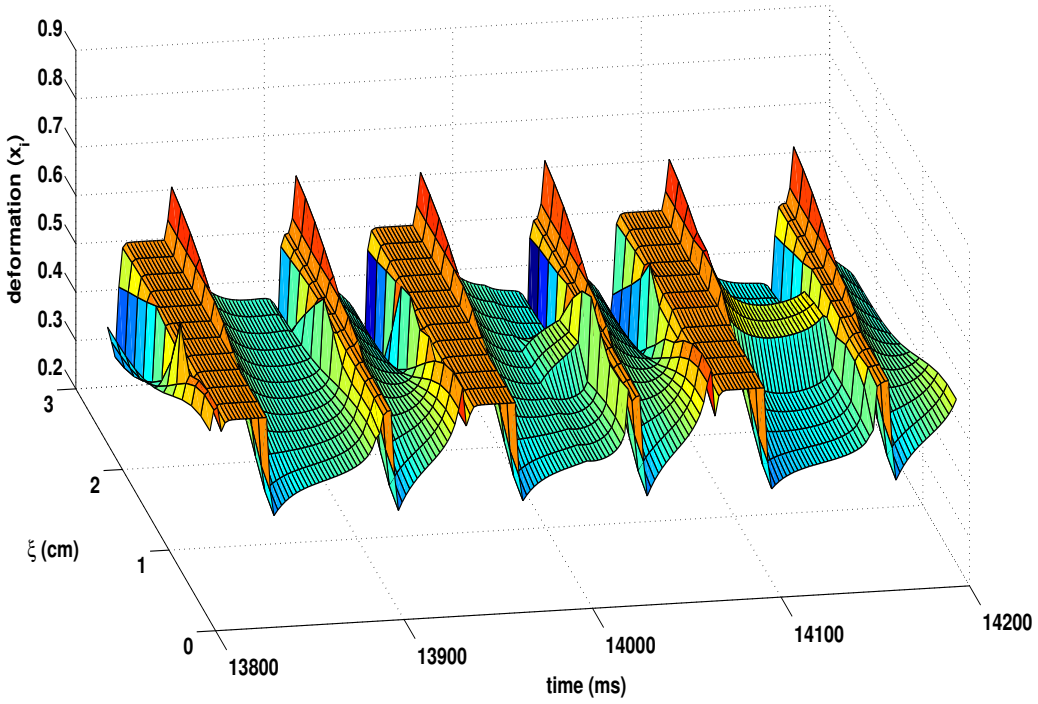

Figure 3.4: Shows the time evolution of the deformation variable x_i. The change in the shape of the curve after 14000 ms is attributed to the action of controller. The sudden expansion at the point of excitation is due to the linear approximation of deformation gradient, F(X).

activated at 14000 ms. Finally, Fig.3.4 shows the action of controller over the region [3, 4.5] cm on the Long (L) - APD.

Thus using a model based on the cardiac mechanics as well as electrophysiology it clearly shows that the electrical APD can be manipulated in order to suppress alternans by using a mechanical based perturbations.

Chapter 4

Conclusions and future work

4.1 Conclusions

This work shows the effectiveness of a controller algorithm that is based on mechanical stimuli along with a boundary pacing control in annihilation of cardiac alternans. The control technique involves mixed algorithm consisting of a electrical based boundary pacing and a electrical independent stimulus (mechanical stimuli) that is spatially distributed along the tissue. Calcium dynamics being identified as the prime component in the electro-mechanic and mechano-electric coupling, effect of its perturbation on alternans stabilization was reported in Chapter.2.

For this study, Luo Rudy-1(LR1), a recently developed model that includes updated currents to numerically reconstruct the depolarization and repolarization of a action potential close to that of a realistic cardiac cell. The cable equation was considered for the transmembrane potential for a tissue of length 6.25 cm with ionic currents as suggested in the LR1 model. The tissue was paced at a frequency so as to induce alternans (discordant). When a boundary pacing control was applied, alternans up to $\approx$ 1 cm of length were suppressed but concordant alternans were developed with increasing amplitude towards the end of the tissue which resulted in a conduction block. Under such a boundary pacing control before the conduction block a spatially distributed calcium controller was initiated. This combined effect of boundary pacing control and a spatially distributed calcium control avoided a conduction block and also suppressed alternans successfully.

The ineffectiveness of a pacing or electrical based boundary control is due to the lack of the information on the instabilities far from the pacing site. A spatially distributed con-

troller actuators provides the controller with this information and aid in annihilation of alternans. This can be explained by the parabolic PDE model discussed in the last section of Chapter.2. The constants in the PDE model are adopted from LR1 ionic model. Analysis on this PDE model provides information on the stable modes, unstable modes and controllability of the system. With longer cardiac tissues the number of unstable modes increases, as in case of a tissue length of 6.25 cm two eigen modes are unstable. A boundary pacing controller has limited controllability and can stabilize the system but only with very high control input, having such a high controller gain is impractical in a real cardiac tissue. This defines the stabilizability of alternans in a real sized cardiac tissue by the suggested control algorithm.

Spatially distributed actuators perturb a chemical species (calcium) in the cells that in effect suppresses the alternans. Calcium dynamics dominate the mechanical contraction in cells. These calcium dynamics also hold the ability to change the APD when affected by a mechanical stimuli. Suppression of alternans by directly manipulation of mechanical stress was reported in Chapter.3. A cardiac tissue of 7 cm was simulated using a simple three variable Nash-Panfilov model with a linear approximation for the deformation gradient. The active tension in the stress-strain model was actuated based on the difference in APD of two consecutive beat in a tissue manifesting alternans. With a change in active tension the deformation gradient, $\mathbf{F}$ is affected which further influences the membrane potential in two ways, as a diffusion term and as current $\mathbf{I_g}$ in the cable equation. Suppression of alternans by perturbing mechanical stress in a model that consists of coupled cardiac electrophysiology and cardiac mechanics supports the results for the controller based on calcium dynamics. Thus the suggested control algorithm that consists of a combined boundary pacing and a spatially distributed mechanical (or chemical species) based controller can effectively annihilate alternans in a real sized cardiac tissue.

4.2 Future Work

In future, annihilation of alternans in a two dimensional NP model by mechanical perturbation can be considered with no approximations on the nonlinear deformation gradient tensor, $\mathbf{F}$. Currently, the procedure adopted in this study involves a linear approximation for

F which limits the maximum contraction in cells to ≈ 8-10 % of the original length. A 2D system of equations as suggested by Whiteley et al. that involves the voltage propagation in two directions whereas the tissue deforms unidirectionally. The governing equations of such a 2D system is given as:

$$F = \begin{bmatrix} x_1'(X1) & 0 \\ 0 & x_2'(X2) \end{bmatrix} \tag{4.1}$$

$$E = \frac{1}{2}\begin{bmatrix} (x_1'(X1))^2 - 1 & 0 \\ 0 & (x_2'(X2))^2 - 1 \end{bmatrix} \tag{4.2}$$

$$C^{-1} = \begin{bmatrix} (2E_{11}+1)^{-1} & 0 \\ 0 & (2E_{22}+1)^{-1} \end{bmatrix} \tag{4.3}$$

The strain energy function in Eq.3.11 is defined in the pole zero form (Whiteley et al., 2007). The strain energy function is defined in terms of the Green-Lagrange strain tensor with the axes aligned with the fibre and fibre sheet, deformation in a direction due to forces and deformation in other directions is affected.

$$W = k_1 \frac{(E_{11})^2}{(a_1 - E_{11})^{b_1}} + k_2 \frac{(E_{22})^2}{(a_2 - E_{22})^{b_2}} \tag{4.4}$$

The stress tensor $T_{MN}^{passive}$ is given as:

$$T_{MN}^{passive} = \begin{bmatrix} \frac{\partial W}{\partial E_{11}} - \frac{p}{2E_{11}+1} & 0 \\ 0 & \frac{\partial W}{\partial E_{22}} - \frac{p}{2E_{22}+1} \end{bmatrix} \tag{4.5}$$

Though the system is two dimensional, the undeformed tissue is subjected to a unidirectional force hence

$$T_{22} = 0 \tag{4.6}$$

To ensure incompressibility of the tissue, detF = detC = 1, and hence the compressibility constraint is given as:

$$(2E_{11}+1)(2E_{22}+1) = 1 \tag{4.7}$$

- Extension of tissue ($E_{11} > 0$, $E_{22} < 0$, $\frac{\partial W}{E_{22}} = 0$)

$$\therefore \quad T_{22} = \frac{-p}{(2E_{22}+1)} = 0, \ \therefore \quad p = 0$$
$$T_{11} = \frac{\partial W}{E_{11}} = k_1 \frac{(E_{11})^2}{(a_1 - E_{11})^{b_1}} \left(2 + \frac{b_1 E_{11}}{(a_1 - E_{11})}\right) \tag{4.8}$$

- Compression of tissue ($E_{11} < 0$, $E_{22} > 0$)

$$\frac{\partial W}{E_{22}} - \frac{p}{(2E_{22}+1)} = 0$$
$$k_1 \frac{(E_{22})^2}{(a_1 - E_{22})^{b_1}} \left(2 + \frac{b_1 E_{22}}{(a_1 - E_{11})}\right) - \frac{p}{(2E_{22}+1)} = 0 \tag{4.9}$$

For a given value of E_{11}, Eqs.4.7 and 4.9 can be solved for E_{22} and p to evaluate

$$T_{11} = -\frac{p}{(2E_{11}+1)} \tag{4.10}$$

Eqs.4.8 and 4.10 give the value of $T_{MN}^{passive}$ for two conditions, extension and conpression of fibre which further can be used to evaluate the deformations. The deformations can be found out by solving the equilibrium relation.

$$\frac{\partial}{\partial X_M} \left(T_{MN} \frac{\partial x_N}{\partial X_N}\right) = 0 \tag{4.11}$$

where x_i and X_i are deformed and undeformed coordinates respectively. As deformations are only in one direction M,N = 1. The electrophysiological model is same as the NP model considered in Chapter.3. Performing simulations in a 2D tissue is a step further in considering a 3D heart with tissue anisotropy.

Bibliography

R. R. Aliev & A. V. Panfilov (1996). 'A simple two-variable model of cardiac excitation'. *Chaos, Solitons & Fractals* **7**(3):293 – 301.

E. Alvarez-Lacalle & B. Echebarria (2009). 'Global coupling in excitable media provides a simplified description of mechanoelectrical feedback in cardiac tissue'. *Phys. Rev. E* **79**(3):031921.

G. W. Beeler & H. Reuter (1977). 'Reconstruction of the action potential of ventricular myocardial fibres'. *Journal of Physiology* **45**:11911202.

D. M. Bers (2001). *Excitation-Contraction Coupling and Cardiac Contractile Force*. Kluwer Academic.

D. M. Bers (2002). 'Cardiac excitation-contraction coupling'. *Nature* **415**(6868):198–205. M3: 10.1038/415198a; 10.1038/415198a.

G. E. Billman (2009). 'Cardiac autonomic neural remodeling and susceptibility to sudden cardiac death: effect of endurance exercise training'. *American Journal of Physiology - Heart and Circulatory Physiology* .

A. Burke & R. Virmani (2005). *SUDDEN NATURAL DEATH — Cardiovascular*, pp. 211–223. Encyclopedia of Forensic and Legal Medicine. Elsevier, Oxford.

S. C. Calaghan, et al. (2003). 'Do stretch-induced changes in intracellular calcium modify the electrical activity of cardiac muscle?'. *Prog. Biophys. Mol. Biol.* **82**:81–95.

D. J. Christini, et al. (2006). 'Control of Electric alternans in Canine Cardiac Purkinje Fibers'. *Phys. Rev. Lett.* **96**:104101.

E. Chudin, et al. (1998). 'Wave propagation in cardiac tissue and effects of intracellular calcium dynamics (computer simulation study)'. *Progress in Biophysics & Molecular Biology* **69**:225–236.

E. Chudin, et al. (1999). 'Intracellular Ca2+ Dynamics and the Stability of Ventricular Tachycardia'. *Biophysical Journal* **77**(6):2930 – 2941.

R. Curtain (1982). 'Finite-dimensional compensator design for parabolic distributed systems with point sensors and boundary input'. *IEEE Trans. Automat. Contr.* **27**:98–104.

S. Dubljevic, et al. (2008). 'Studies on feedback control of cardiac alternans'. *Computers and Chemical Engineering* **32**(9):2086 – 2098.

B. Echebarria & A. Karma (2002). 'Spatiotemporal control of cardiac alternans'. *Chaos* **12**:923–930.

R. FitzHugh (1961). 'Impulses and physilogical states in theoretical models of nerve membrane'. *Biophysical J* **1**.

J. J. Fox, et al. (2002). 'Spatiotemporal Transition to Conduction Block in Canine Ventricle'. *Circ. Res.* **289**.

A. Friedman (1976). *Partial Differential Equations*. Holt, Rinehart & Winston, New York.

A. Hodgkin, AL. Huxley (1952). 'A quantitative description of membrane current and its application to conduction and excitation in nerve'. *J Physiol (Lond)* **117**:500–544.

P. Kohl, et al. (1999). 'Stretch-induced changes in heart rate and rhythm: clinical observations, experiments and mathematical models'. *Prog. Biophys. Mol. Biol.* **82**:91–138.

M. Lab & J. Lee (1990). 'Changes in intracellular calcium during mechanical alternans in isolated ferret ventricular muscle'. *Circ Res* **66**(3):585–595.

S.-F. Lin & S. Dubljevic (2007). 'Pacing Real-Time Spatiotemporal Control of Cardiac Alternans'. In *American Control Conference, 2007. ACC '07*, pp. 600 –606.

C. Luo & Y. Rudy (1994a). 'A dynamic model of the cardiac ventricular action potential. I. Simulations of ionic currents and concentration changes'. *Circ Res* **74**(6):1071–1096.

C. Luo & Y. Rudy (1994b). 'A dynamic model of the cardiac ventricular action potential. II. Afterdepolarizations, triggered activity, and potentiation'. *Circ Res* **74**(6):1097–1113.

C.-H. Luo & Y. Rudy (1991). 'A model of the ventricular cardiac action potential:depolarization, repolarization, and their innteraction'. *Circulation Research* **68**:15011526.

L. Makarov & V. Komoliatova (2010). 'Microvolt T-Wave Alternans during Holter Monitoring in Children and Adolescents'. *Annals of Noninvasive Electrocardiology* **15**(2):138–144.

S. M. Narayan (2007). 'T-Wave Alternans and Human Ventricular Arrhythmias: What Is the Link?'. *J Am Coll Cardiol* **49**(3):347–349.

M. P. Nash & A. V. Panfilov (2004). 'Electromechanical model of excitable tissue to study reentrant cardiac arrhythmias'. *Progress in Biophysics and Molecular Biology* **85**(2-3):501 – 522. Modelling Cellular and Tissue Function.

S. A. Niederer, et al. (2006). 'A Quantitative Analysis of Cardiac Myocyte Relaxation: A Simulation Study'. *Biophysical journal* **90**(5):1697–1722.

D. Noble (1962). 'A Modification of the Hodgkin-Huxley Equations Applicable to Purkinje Fibre Action and Pace-Maker Potentials'. *J. Physiol.* **160**:317–352.

J. M. Pastore, et al. (1999a). 'Mechanism Linking T-Wave Alternans to the Genesis of Cardiac Fibrillation'. *Circulation* **99**(10):1385–1394. http://circ.ahajournals.org/cgi/reprint/99/10/1385.pdf.

J. M. Pastore, et al. (1999b). 'Mechanism linking T-wave alternans to the genesis of cardiac fibrillation'. *Circ.* **99**:1385–1394.

E. Patterson, SW. Starling (1914). 'On the mechanical factors which determine the output of the ventricle'. *J Physiol (Lond)* **48**:357–379.

W. H. Ray (1981). *Advanced Process Control*. McGraw-Hill, New York.

Y. Shiferaw & A. Karma (2006). 'Turing instability mediated by voltage and calcium diffusion in paced cardiac cells'. *Proceedings of the National Academy of Sciences* **103**(15):5670–5675.

O. E. Solovyova, et al. (2004). 'Mathematical modeling of mechano-electric feedback in cardiomyocytes'. *Russ. J. Numer. Anal. Math. Modelling* **4**:331–351.

E. Starling (1918). *The Linacre Lecture on the Law of the Heart*. Longmans, Green and Co, London.

J. Whiteley, et al. (2007). 'Soft Tissue Modelling of Cardiac Fibres for Use in Coupled Mechano-Electric Simulations'. *Bulletin of Mathematical Biology* **69**:2199–2225. 10.1007/s11538-007-9213-1.